
# Design Assesment of the Sawing Wire System Used in Salvage Operations

M. Huisman

Technische Universiteit Delft

TU Delft

# Thesis report

# Design Assessment Of The Sawing Wire System Used In Salvage Operations

by

M. Huisman

to obtain the degree of Master of Science
at the Delft University of Technology,



| | | |
|---|---|---|
| Student number: | 4281535 | |
| Project duration: | December, 2015 – September, 2016 | |
| Thesis committee: | Prof. Dr.. Metrikine, | TU Delft |
| | Dr.ir. K.N. van Dalen | TU Delft |
| | Ir. C. Keijdener | TU Delft |
| | Ir. P. Antonakas | Boskalis |
| | Ir. P. Hendrickx | Boskalis |

# Summary

The Smit sawing wire system was used in the salvage operation of the Baltic Ace. The sawing wire was drilled underneath the wreck and connected to two barges on opposite sides. Winches were placed on the barges to make a controlled cut through the wreck by pulling the sawing wire back and forth. The cut was made in an upward direction as shown in figure 1. While the sawing wire was pulled in by one winch, the winch on the other side kept a holding tension on the sawing wire to create a normal force in the wreck. This normal force was necessary to make the cut through abrasive wear. To get a better insight into the forces experienced in the sawing wire system, measurements were conducted during the cutting operations. The objective of this research project is to contribute to the assessment of the sawing wire system, by providing a simulation model based on theory and compare this with measurements of the salvage operation of the Baltic Ace. The measurements show a peak tension at the beginning of the sawing cycle that was not expected in calculations made prior to the operation. In friction theory, this is called the breakaway force that is needed to get the sawing wire moving. The breakaway force is caused by the difference in static and kinetic friction coefficients between the sawing wire and the wreck.

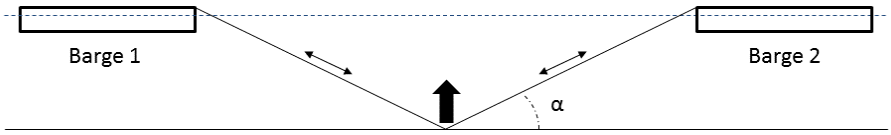


Figure 1: Barge position

The simulation model is made in Orcaflex and includes the friction at the contact points, barge movement, and the heave compensators. The friction is included by a Coulomb friction model for the kinetic friction, a tension for the breakaway force and a stick-slip damper for the intermittent motion of the wire. The heave compensator stroke is controlled by a code in python that measures the sawing wire angle and the heave motion of the barges at the fairlead position. The barge motions were included by force-RAO's, calculated in AQWA. The wave environmental forces are simulated using a JONSWAP spectrum with the wave height and period similar to those during the sawing operation. After completion of the model, the results were compared with the measurements. The tension graph of the model has similar peak forces at the beginning of the cycle (first 10s.) and similar lower force fluctuations in the constant part (10-50 s.). These results together with the comparison in the frequency domain are used to verify the model, hereafter the model is considered correct and ready for use in future sawing calculations.

The design of the sawing wire system is assessed for implementation in future operations. The assessment includes the effect of the heave compensators, the influence of the friction force concerning a larger or smaller diameter wreck and the elimination of the peak tension. Simulations show that the heave compensator has no effect on the peak tension located at the beginning of the sawing cycle. Though some recommendations are given for the case when lower fluctuation of the tension is required. Simulations show an increase of the compensation effect when the declination angle $\alpha$ is changed from 20 to 30 degrees, by placing the barges closer together. Both the bending of the steel cable inside of the surrounding bushes and the required lateral forces limit the increase of the declination angle. Secondly, it is advised to extend the controller of the motion compensation by including the horizontal motions of the barges, resulting in lower tension fluctuations in the sawing wire. Furthermore, calculations of the friction force for a different diameter wreck result in lower forces for a smaller diameter wreck. With lower forces in the system, the required power is also smaller. Alternatively, for a bigger wreck the fiction forces and required power will be higher. Furthermore, theory shows that the peak tension can be eliminated if lower maximum forces in the system are desired. This is done by lowering the holding force at the start of the sawing cycle and raising the tension in the kinematic stage with a PID controller.

# Acknowledgement

Without the help of some people, the completion of my thesis would have been impossible. Therefore, I would like to explicitly thank them here for their help and guidance during the entire process.

First of all, I would like to thank my supervisors at Boskalis: Panagiotis Antonakas and Peter Hendrickx. Panagiotis you guided me through the project and showed great interest in my work during the many meeting we had. Peter you also helped me throughout the project but especially when Panagiotis was away offshore.

From the TU-Delft I would like to thank: Chris Keijdener, my daily supervisor. Your experience in modeling of dynamic problems turned out to be very helpful in finding my way during my thesis research. I would also like to thank my professor: Andrei Metrikine. In the few meetings we had you always showed great interest in the topic and was eager to help me find the best way to solve the problems.

I would like to thank my family and friends. Your support throughout my entire study made is possible to be where I am today. My parents: Elly Augustinus and Victor Huisman, for making it possible for me to study. Frank Sterke, Wouter van Zoest, with whom I had the privilege to start studying and Wouter Molenbroek and Steven Hannink who helped me shape who I am today.

*M. Huisman*
*Delft, September 2016*

# Contents

**Summary** iii

**Acknowledgement** v

**List of Figures** ix

**List of Tables** xi

**1 Introduction** 1
- 1.1 Salvage Market . . . 1
- 1.2 The Smit sawing wire system . . . 1
- 1.3 The Baltic Ace salvage operation . . . 2
- 1.4 Thesis objective . . . 3
- 1.5 Methodology . . . 4

**2 Measurements** 5
- 2.1 Time domain . . . 5
- 2.2 Frequency domain . . . 7
- 2.3 Conclusions . . . 8

**3 Background Theory** 9
- 3.1 Friction . . . 9
  - 3.1.1 Stick-Slip Phenomenon . . . 12
  - 3.1.2 Friction models . . . 13
- 3.2 Abrasive Friction and Wear . . . 15
- 3.3 Inertia . . . 16
- 3.4 Heave Compensator . . . 16
- 3.5 Conclusions . . . 16

**4 Model** 17
- 4.1 Barges . . . 18
- 4.2 Sawing wire . . . 19
- 4.3 Friction model . . . 20
- 4.4 Winch set-up . . . 21
- 4.5 Heave compensator . . . 22
- 4.6 Environmental input data . . . 23
- 4.7 Simulation Results . . . 24
- 4.8 Conclusions . . . 26

**5 Comparing the Results** 27
- 5.1 Time Domain Comparison . . . 27
- 5.2 Frequency Domain Comparison . . . 29
- 5.3 Heave Compensator . . . 29
- 5.4 Conclusions . . . 32

**6 Design Assessment** 33
- 6.1 Accidental load scenario's . . . 33
  - 6.1.1 Winch settings . . . 33
- 6.2 Future implementation of the system . . . 35
  - 6.2.1 Different diameter - monopile/costa concordia . . . 35
  - 6.2.2 Different material - tunnel . . . 36
- 6.3 Eliminating The Peak Friction Force . . . 36
  - 6.3.1 Friction Compensation With PD control . . . 37

6.4 Influence of the Heave Compensator . . . 37
6.5 Conclusions. . . . 39

**7 Conclusions and recommendations 41**
7.1 Conclusions. . . . 41
7.2 Recommendations . . . 42

**A Appendix-A 43**

**B Appendix-B 47**

**C Appendix-C 51**

**D Appendix-D 53**

**Bibliography 61**

# List of Figures


1 Barge position . . . iii

1.1 Barge position . . . 1
1.2 Bushes on the wire . . . 2
1.3 Location of wreck . . . 2

2.1 Sawing wire tension . . . 5
2.2 Sawing wire velocity . . . 6
2.3 Long measurement tension . . . 6
2.4 Tension sawing wire . . . 7
2.5 Heave cylinder pressure . . . 8

3.1 Schematic of the forces need to move two bodies, with relative definition of static and kinetic friction from Straffelini [17] . . . 9
3.2 Peak Tension Compared to Velocity . . . 10
3.3 Velocity dependent coefficient of friction adopted from Straffelini [17] with data from Bhushan [2] and Briscoe [6] . . . 10
3.4 Force equilibrium . . . 11
3.5 Friction coefficient from measurements . . . 11
3.6 Stick slip example . . . 12
3.7 1-DOF model with dry friction . . . 13
3.8 Stribeck friction model . . . 14
3.9 Friction coefficient . . . 15
3.10 Stick-Slip tension . . . 15
3.11 Heave compensator set-up . . . 16

4.1 Overview of the model . . . 17
4.2 Rounding of the corners . . . 17
4.3 RAO Stemat barge . . . 18
4.4 Sawing wire assembly . . . 19
4.5 Bush dimensions . . . 19
4.6 Friction shape . . . 20
4.7 Stick-Slip Damper . . . 21
4.8 Winch setting . . . 21
4.9 Constant tension . . . 22
4.10 Influence pitch and yaw . . . 23
4.11 Environmental Measurements . . . 23
4.12 Frequency spectrum . . . 24
4.13 Direction Spectrum . . . 24
4.14 Tension of right winch . . . 25
4.15 Velocity of right winch . . . 25
4.16 Tension of right winch . . . 26

5.1 Tension comparison . . . 27
5.2 Tension comparison . . . 28
5.3 Tension comparison . . . 28
5.4 Comparison of tension in Frequency domain . . . 29
5.5 Heave compensator effect left . . . 29
5.6 Heave compensator effect right . . . 30

5.7 Heave compensator effect left . . . 30
5.8 Heave compensator effect right . . . 31
5.9 Barge Motion in Surge . . . 31
5.10 Barge Motion in Heave . . . 32

6.1 Power needed to get both the tension and velocity . . . 34
6.2 Some scenarios for next use of the cutting wire system . . . 35
6.3 Friction block . . . 35
6.4 Tension Without Peak . . . 36
6.5 Heave Influence for Different Angles . . . 37
6.6 Influence of heave and surge . . . 38
6.7 Barge Velocity Surge/Heave . . . 39
6.8 Bending of the wire inside bushes . . . 39

C.1 heave compensator scheme . . . 52

D.1 Stemat 89 . . . 56
D.2 MSB3301 . . . 57
D.3 RAO Stemat barge . . . 58
D.4 RAO Stemat barge . . . 59

# List of Tables

4.1 Geometry of the barges . . . . . 18
4.2 Settings Heave Compensator . . . . . 22

6.1 Accidental load cases . . . . . 33
6.2 Winch Settings from Huisman Equipment [11] . . . . . 34
6.3 Influence Heave Compensator . . . . . 38

A.1 Left winch settings . . . . . 44
A.2 Right winch settings . . . . . 44
A.3 Left Tensioner settings . . . . . 45
A.4 Right Tensioner settings . . . . . 45

D.1 Specifications Stemat 89 . . . . . 56
D.2 Specifications MSB3301 . . . . . 57

# Nomenclature

**Number Sets**

| | |
|---|---|
| $Hz$ | $Hertz = s^{-1}$ |
| $H_s$ | Significant wave height |
| $T_s$ | Significant wave period |
| $\mu$ | Friction Coefficient |
| $F_c$ | Coulomb friction force |
| $k_v$ | Sliding Coefficient |
| QTF | Quadratic transfer function |
| RAO | Response Amplitude Operator |
| Te | Tonne |

**Physics Constants**

| | |
|---|---|
| $g$ | Gravitational Constant |
| $Kxx$ | Radius of gyration about x axis |
| $Kxx$ | Radius of gyration about x axis |
| $Kyy$ | Radius of gyration about y axis |
| $Kyy$ | Radius of gyration about y axis |
| $Kzz$ | Radius of gyration about z axis |
| $Kzz$ | Radius of gyration about z axis |
| $N$ | Normal Force |
| $r$ | arm length [m] |
| $v$ | Velocity |
| $W$ | Watt |
| $\omega$ | Angular velocity [rad/s] |
| $\pi$ | 3,141.. |
| $e$ | Euler's number (2.71828..) |
| i | Imaginary number |

# 1 Introduction

## 1.1. Salvage Market

Boskalis/Smit specializes in the salvage operations around the world. These include the removal of wrecks, extracting hazardous fuels from sinking ships and the rescue of ships in trouble. In this thesis the focus lies on the wreck removal aspect of the salvage market. In most cases a wreck can be made buoyant and towed back to a sheltered harbor, but in some cases the wreck is damaged such that is is impossible to make it buoyant again and therefore it will need to be salvaged in place. In these cases a crane vessels or barges is required to remove the wreck. In the case discussed in this thesis the wreck is too heavy to be lifted in one piece and is therefore cut into smaller pieces.

## 1.2. The Smit sawing wire system

The sawing wire system used for salvage operations is similar to a wire saw. The wire is around 100 meter in length and is pulled back and forth by two winches. The first step in the cutting operation is to drill the sawing wire from one side, passing underneath the wreck and connecting it to the other side. Once it is connected to the two winches on both sides the sawing can commence and a cut is made in vertical direction upward, as illustrated in figure 1.1.

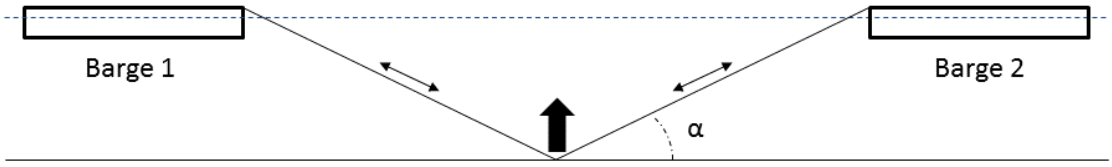


Figure 1.1: Barge position

Small cylinder bushes of $0.112m$ in length, with a hole in the middle are slided over the wire to be fixed in place. The bushes are fixed under pre-tension, by elongation of the wire before placement of the fixing bolts at both ends. A picture of the bushes that are slided over the wire is seen in figure 1.2. On the outside of the bushes, pieces of hard metal are soldered to give it a roughness that will make the cut in the wreck.

The cutting wire technique was previously used for the salvage of the Russian submarine The Kursk in the Barents Sea and for the car carrier MV Tricolor in the English Channel. In the salvage operation of the Kursk, the sawing wire system was used to make a cut just behind the front section of the submarine where the explosives were placed. In this operation, the sawing wire system was placed on the seabed. The sawing wire movement was made by two large cylinders and the cut was made vertically downward. The MV Tricolor was cut into several pieces during its salvage operation, the separate pieces of the wreck were later lifted from the seabed. In this salvage operation, the sawing wire system was operated from two jack-up barges that were able to lift them-self out of the water on four legs. The sawing wire was drilled underneath the wreck and the cutting of the wreck commenced in an upward cut just as described before.

Figure 1.2: Bushes on the wire

## 1.3. The Baltic Ace salvage operation

In December 2012 the Baltic Ace, a Roll-on Roll-off vessel, collided with the Corvus J. in the North Sea. Due to the damage on the side of the Baltic Ace, she sank to the bottom of the North Sea. The incident took place only 40-50 kilometers from the port of Zeebrugge where she left, bound for Finland. The ship lay on her side in the channel at a depth of 35 meters, only 10-12 meters from the surface. Since the ship lay on one of the busiest shipping lanes in the world, it was considered to be a potential hazard to other vessels. The location is shown in figure 1.3


Figure 1.3: Location of wreck

The removal of the Baltic Ace wreck has been executed by Boskalis and its partner Mammoet Salvage. In an early stage it became apparent that the ship could not be salvaged intact and it was decided to cut it into several smaller sections. This cutting was done with the use of the SMIT sawing wire system. Due to the extremely bad condition of the ship, it became clear that that the six pieces of the original plan were too heavy to be lifted. Eventually, the Baltic Ace wreck was cut into eight pieces, which were lifted separately from the North Sea floor. This thesis will focus on this salvage case since measurements were taken during the operation that can be used to validate and compare the model.

## 1.4. Thesis objective

This thesis can be described as a diagnostic research, where a background analysis is needed to find the cause of a problem. The problem and objective of the thesis are described next.

**Problem:** Assumptions were made prior to the salvage operation of the Baltic Ace, most of these assumptions concerned the friction of the sawing wire in the wreck. In order to completely understand this friction, measurements were taken during the operation. In the measurements it became apparent that there are peak tension forces in the wire that were not expected in calculations made prior to the operation.

The existing theories and knowledge within Boskalis cannot adequately indicate which of the many possible factors have influenced this problem. It is also not known whether particular factors have caused the entire problem or only a specific part of it.

**Objective:** The objective of this research project is to contribute to the assessment of the sawing wire system regarding the friction, by providing a simulation model based on theory and compare this with measurements of a salvage operation.

The practical relevance of the project is to gain knowledge in the salvage operations, which is done by answering the following research questions.

**Central research questions**
1. Where do the high tension peaks at the beginning of a cut originate from?
2. What is the friction coefficient that can be used for the simulation of a shipwreck?
3. How can we include different friction coefficients in a model?

**Sub-questions**
- What is stick-slip friction and is this present?
- What is the influence of inertia in the system?
- How is the heave motion of the barges compensated?
- What information is shown in frequency domain analysis of the measurements?

## 1.5. Methodology

The measurements that were taken during the salvage operation consist of large files of signals made with a prescribed interval. Before the measurement data could be analyzed, the data needed to be processed further. The data was analyzed for different cuts of the wreck. In most of the tension data, the big tension peak was measured and the main focus of interest converged to this observed tension peak.

The method used to find the origin of the big tension peak is a comparative approach, in which a model based on theory will be compared with the measurements. Both time domain and frequency domain comparison would give interesting information and could be used to validate the model.

When the source of the big tension peak is found the sawing wire system should be assessed to provide enhancement of the system. If the source of the peak is found it might be possible to recommend an action to be taken for this peak tension to be eliminated. Another thing that was frequently asked of this research is to discuss the influence of the heave compensator, which some of the people involved found to be of little effect to the operation.

It is considered to be a good approach to make a simulation model similar to the operation to assess the origin of the peak tension that was measured. Besides the actual research into the peak tension, the simulation model will provide extensive knowledge into the working of the sawing operation.

# 2

# Measurements

The measurements made during the salvage operations include amongst others barge motions, the tension in the sawing wire, the velocity of the winches and pressure in the heave compensator cylinder. The vast amount of data is analyzed to gain a better understanding of the operation and acknowledge unexpected behavior. The model of the operation is later validated with use of these measurements. The metocean data measured during the operation can be reproduced as input to the model, which contributes to its accuracy.

The first step in this chapter is the time domain analysis to show the sawing cycles. Thereafter the measurements are transformed into the frequency domain to discover the peak frequencies in the system.

## 2.1. Time domain

The cutting of one section of the wreck generally takes around 30 hours. The sawing cycles, pulling in wire until the winch directions are changed, have a duration of around 50 seconds. There is a stop of 5 seconds between the change of direction to lower the tension in the system. In figure 2.1 the tension in the sawing wire is shown. Points of interest are the overshoot peaks in the tension force at the beginning of a sawing cycle, these overshoots can be a lot higher than the average tension peaks (range of 20-30 percent). The high peaks are the single most important phenomenon discussed in this research.

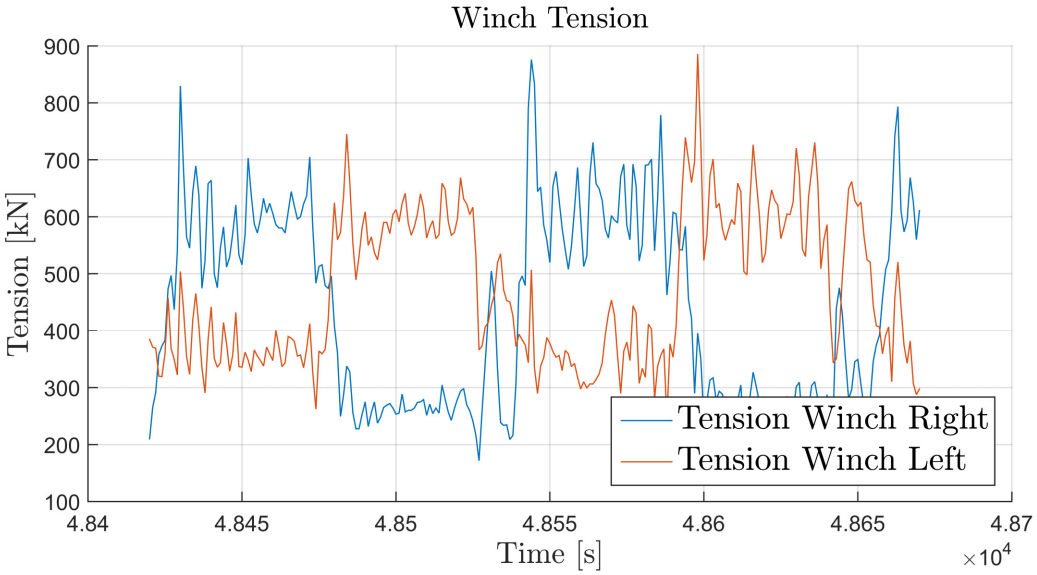


Figure 2.1: Sawing wire tension

In figure 2.2 the velocity of the winch pay-out of sawing wire is shown. In the velocity graph, the negative velocity indicates that the winch is hauling in the sawing wire. It can be seen that the speed is kept at a nice constant velocity setpoint when pulling in the wire, though the paying-out parts are more irregular.

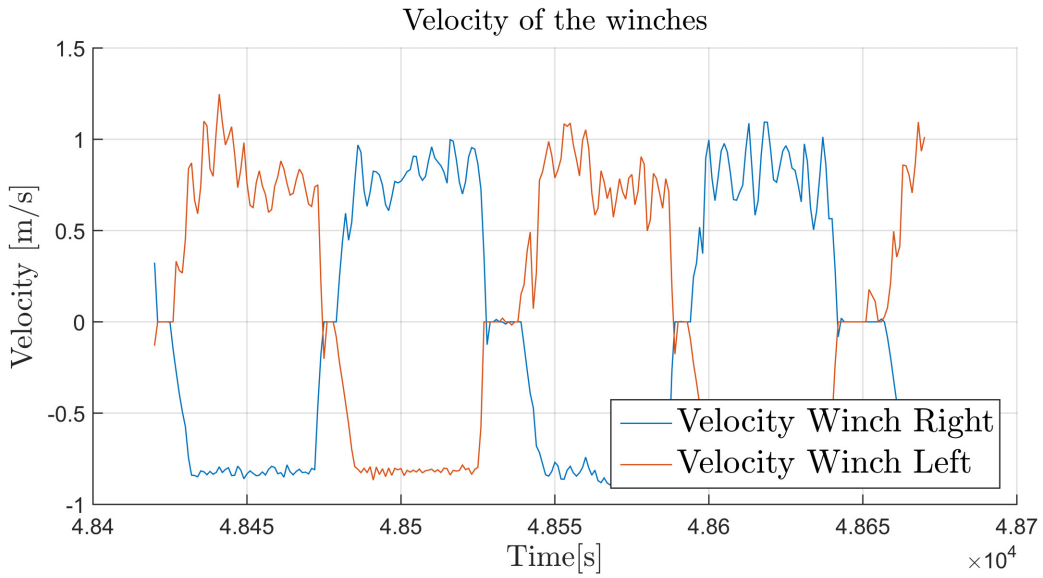


Figure 2.2: Sawing wire velocity

In figure 2.3 the tension at both winches is shown for a longer time period. The overshoot in the tension force is not seen at every sawing cycle in the figure and they occur mostly in measurements of the Stemat barge (Left Winch).

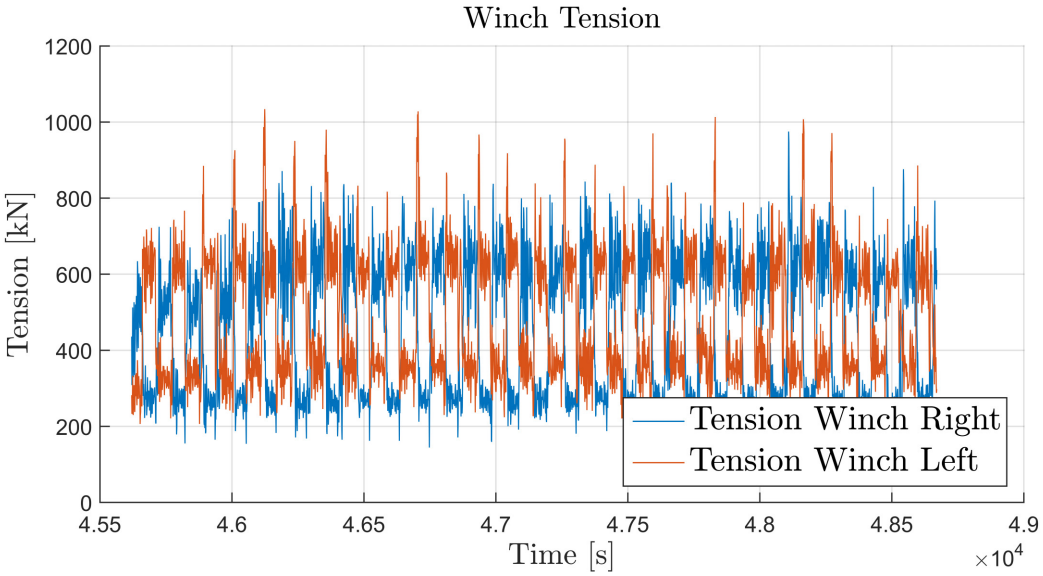


Figure 2.3: Long measurement tension

## 2.2. Frequency domain

The measurements were made in the time domain, in which the value of a sensor is captured with a certain sampling frequency (Fs, logging). By making use of the Fourier transformation, the values can be converted from the time domain to the frequency domain as described in more detail later. By doing this, measurements which occur with a certain frequency are added together. In the Fast Fourier Transform (FFT) these measurements result as peaks in the spectrum. As a result, a clear distinction can be made between the common frequencies. This can be used to clarify the forces measured in the system.

The time domain measurements are converted to the frequency domain with the use of the following equation from Osgood [15].

$$F_f = \int e^{-2\pi i x} f(x) dx \tag{2.1}$$

This calculation is done for each time step in Matlab using the FFT function. The Nyquist frequency is the maximum resolvable frequency for a data set similar to half the sampling frequency, $f_{max} = \frac{Fs}{2}$. This is often called the Shannon Sampling Theorem as described in Osgood [15]. All frequencies higher than the Nyquist frequency are added to the lower frequencies, which causes a small error, this is called Aliasing. The sampling frequency of the data set used is 1 Hz and the frequency range of interest is 0 to 0.3 Hz. Due to the Nyquist frequency the signal will be cut off the for frequencies higher than $0.5Hz$ (periods lower 2 seconds). Also due to the low sampling frequency of 1 Hz some of the higher frequencies might not be covered and information might be lost, but this is not considered to be of interest for this system.

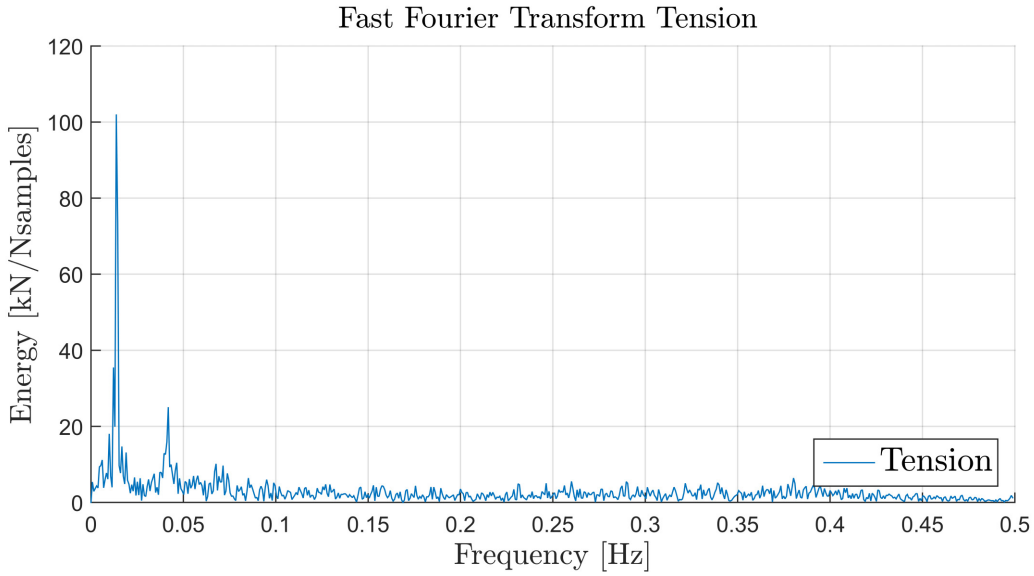


Figure 2.4: Tension sawing wire

In figure 2.4 and 2.5 the frequency domain plots are shown for tension in the sawing wire and the pressure in the heave compensator. The signal used to make these graphs is the normalized amplitude of the tension signal. This signal is divided by the number of samples to get the results. Furthermore, the separate FFT's of five consecutive time samples of 200 seconds were taken and the results were added together. This is done to get more accurate average values over a larger period of time.

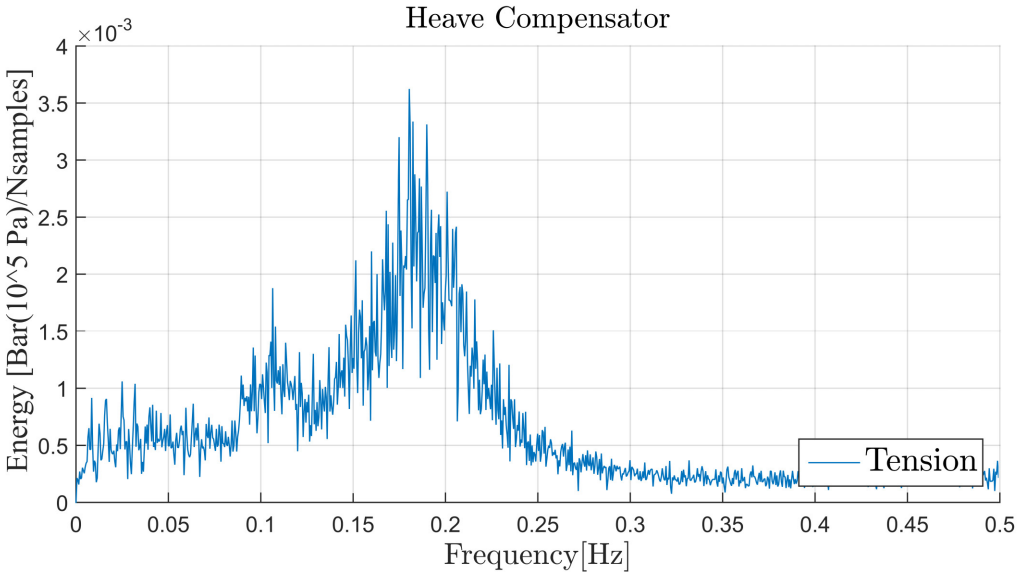


Figure 2.5: Heave cylinder pressure

The first big peak in figure 2.4 is considered to be the influence of the sawing wire cycles, moving back and forth in 100 seconds with a peak at the beginning. The heave compensator pressure in figure 2.5 naturally finds a peak in the range of frequency similar to the $1^{st}$ order waves that influence the heave motions of the barge. The period of the $1^{st}$ order waves in the north sea are generally in the range of 3-7 seconds, which is equal to a frequency of $0.145 - 0.33[Hz]$.

In a later stage of this thesis, these results are used to validate the model and to conclude about the origin of peak forces.

## 2.3. Conclusions

The measurements of the sawing wire operation show peak tensions in the beginning of a sawing cycle. These tensions are present most of the time but not always. The velocity of the sawing wire is very constant during the hauling in of the wire but varies a lot during pay-out. The frequency domain analysis of the tension in the sawing wire shows peaks at 0.01 and 0.04 seconds. These peaks show the energy or the number of times peaks occur at a similar frequency. The first peak is considered to be the sawing cycle of the sawing wire moving back and forth (100 sec.) and the second peak is considered to be the lower tension fluctuations seen in the measurements (25 sec.). The frequency domain plot of the heave compensators shows a peak at the first order wave frequencies.

# 3

# Background Theory

This chapter describes the theory that is necessary to understand the cutting process of the sawing wire system. The most important part of this chapter is the friction between the surface of the wreck and the sawing wire. The friction is needed for the sawing wire to wear down the steel of the wreck and cut through it. Another important part of this chapter is the theory of the heave compensators that are placed on the barges during the sawing operations.

## 3.1. Friction

Two bodies kept together by a normal force as shown in figure 3.1a require a tangential force $F_t$ in order to generate a movement between them. This force is called the friction force and it is required to overcome the static friction force $F_f$. As described by Straffelini [17] the ratio between the *tangential force* $F_t$ and the *static friction force* $F_f$ is called the friction coefficient, $\frac{F_t}{F_f} = \mu_s$. This friction coefficient is mostly dependent on the normal force applied and the surfaces of the bodies.

When there is a constant movement between the two bodies similar to the movement of the sawing wire through the wreck, one body has a sliding speed with respect to the other body. In order for this constant velocity to occur the tangential force needs to overcome the dynamic friction force. The ratio between the *tangential force* $F_t$ and the *dynamic friction force* $F_f$ is given by: $\frac{F_t}{F_f} = \mu$. This coefficient of dynamic (or kinetic) friction is dependent on the normal force and the velocity. The static friction force is generally higher than the dynamic friction force, an example of this is given in figure 3.1b. Generally, the difference between the static and dynamic friction is around $20-30\%$ as described by Straffelini [17].

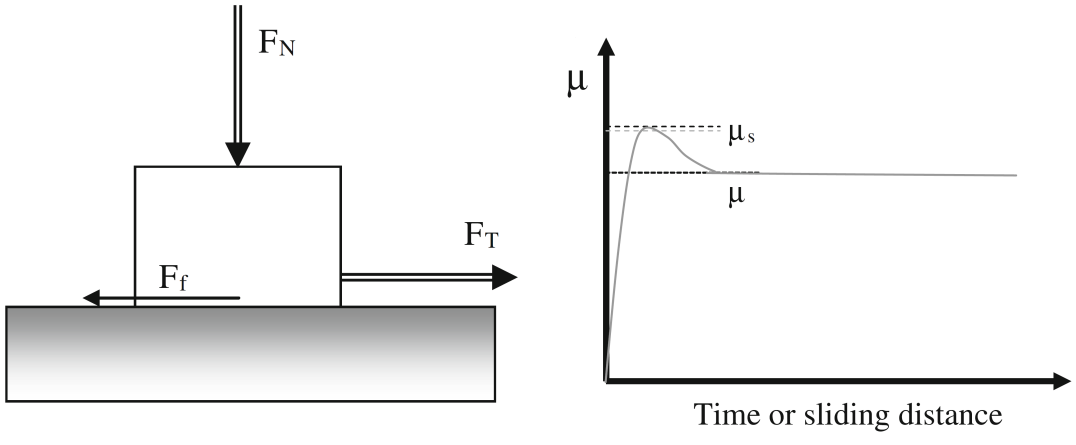


(a) (b)

Figure 3.1: Schematic of the forces need to move two bodies, with relative definition of static and kinetic friction from Straffelini [17]

The graph of the tension measurements taking during the cutting operation is shown in figure 3.2, together with the velocity of the winch. It can be seen that the difference in tension between the first peak of a cycle and the kinetic stage of the sawing cycle is around 20 – 30%, similar to theory. Another point to notice in figure 3.2 is the rise in tension which already happens before the sawing wire is moving. Also, the peak tension is present before the velocity set-point of 0.8$[m/s]$ is reached. Considering this and the consistent occurrence of the peak, it is reasonable to assume that the first peak is present due to the difference in static and dynamic friction coefficients which is the called breakaway force.

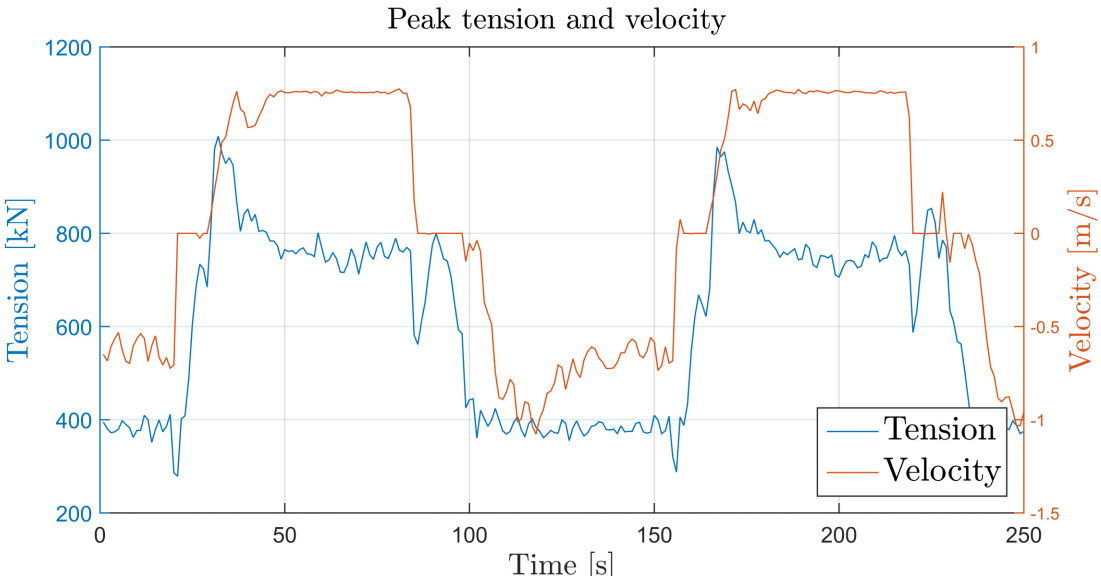


Figure 3.2: Peak Tension Compared to Velocity

The influence of the velocity to the friction coefficient of a two-body system is shown in figure 3.3. The graph of 'High-strength steel' represents similar characteristics as the wreck. The graph shows lower coefficients of friction for higher velocities. The set-point for the sawing wire of 0.8$[m/s]$ results in a coefficient of friction close to 0.75. The value of the friction coefficient is also approximated with formula 3.1 found by Straffelini [17]. This formula results in a friction coefficient of 0.809. The measured friction coefficient is discussed next.

$$\mu = 0.78 - 0.13 \cdot Log_{10}(v) \tag{3.1}$$

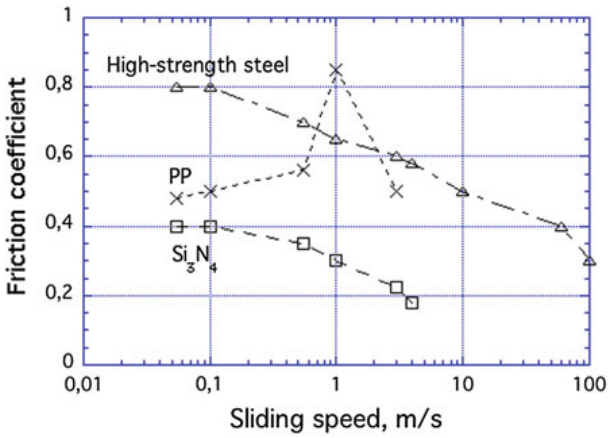


Figure 3.3: Velocity dependent coefficient of friction adopted from Straffelini [17] with data from Bhushan [2] and Briscoe [6]

For the sawing wire system the lateral and normal forces are described by the statistics seen in figure 3.4.

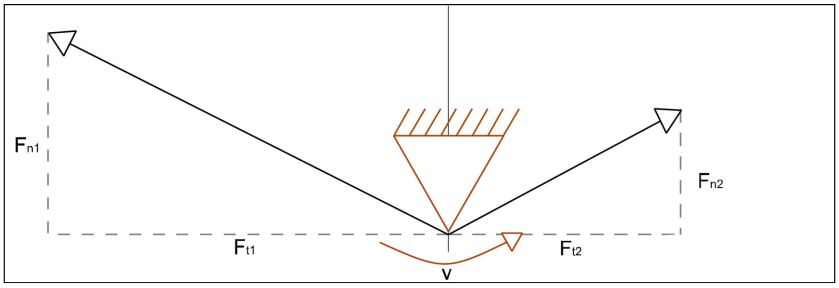


Figure 3.4: Force equilibrium

Where the normal force is calculated as:

$$F_N = sin(\theta_1)F_1 + sin(\theta_2)F_2 \tag{3.2}$$

The lateral force is calculated as:

$$F_L = -cos(\theta_1)F_1 + cos(\theta_2)F_2 \tag{3.3}$$

Equations 3.2 and 3.3 are used to calculate the friction coefficient of the wreck. The tension measured at the winches and the angle of the sawing wires going to the wreck are measured for each time step. As described before, the friction coefficient is calculated as, $\mu = \frac{F_L}{F_N}$. The resulting friction coefficient for these measurements is shown in figure 3.5. It is clear that the coefficient is higher at the beginning, at the location of the peak tension. This value is close to 1 and the sliding friction is around 0.8, which is similar to the theory described earlier.

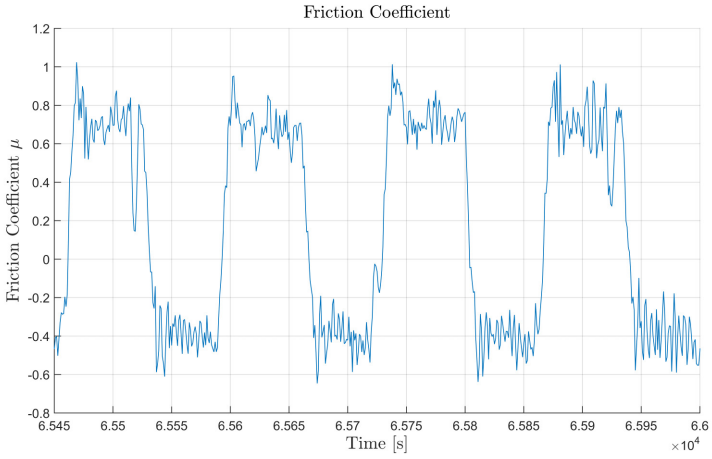


Figure 3.5: Friction coefficient from measurements

Assuming a constant pulling force $F_1 = 700kN$ and a holding force of $F_2 = 300kN$, resulting in a normal force of $F_N = 422kN$. The weight of the sawing wire of $36.2kN$ is subtracted, a resulting normal force $F_N = 385.8kN$. The wreck of the Baltic Ace is around 25 meters in width and similar height, therefore the length of the contact between the sawing wire and a deck of the wreck is assumed to be $20[m]$. The bushes have a diameter of $0.108[m]$ as shown later in figure 4.5.

$$F_{static} = F_N \cdot Length \cdot Diameter \cdot \mu_s \tag{3.4}$$

$$F_{dynamic} = F_N \cdot Length \cdot Diameter \cdot \mu_d \tag{3.5}$$

Resulting from these equations is a static force of $950.6kN$ and a dynamic force of $691.4kN$. The difference

between static and dynamic force is around $258.5kN$. This is approximately similar to the difference between the first high tension peak and the constant part of the rest of the cut as shown in measurements of figure 3.2. This difference is in the range of $20-30\%$ as described before.

### 3.1.1. Stick-Slip Phenomenon

The static friction is generally higher than the dynamic friction due to a relaxation of the material and therefore a better connection between two surfaces. This is described in Straffelini [17] as "an increase of the real area of contact which allows the adhesive force to fully develop". When the static friction is higher than the dynamic friction the phenomenon of stick-slip friction may occur.
The friction force that is needed to *make the body move* is higher than the force that is needed to *keep the body moving*. Therefore at low velocity, it is possible for the system to fall back into the static state. Since the stick and slip forces are continuously interchanged the system experiences an intermittent motion. This can be described as a change of friction coefficient around a mean. The resulting effect can be seen in figure 3.6. The sawing wire is known to have some kind of intermittent motions but this may also be present due to the sliding of the bushes past a ridge in the wreck. It is expected that the full static friction is not present after the sawing wire is moving, since the tension graph of figure 3.2 looks more like graph A than graph B of figure 3.6, thus showing a big peak in the beginning.

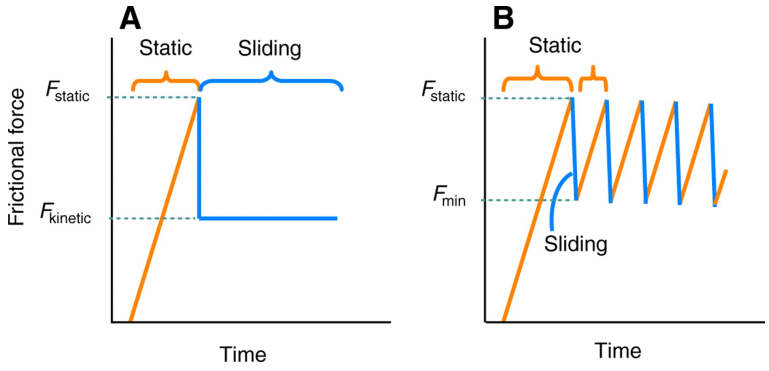


Figure 3.6: Stick slip example

The stick-slip phenomenon can best be described by the example treated in van Campen et al. [19] and Van de Vrande, B. L., Van Campen, D.H., and De Kraker [20] which is based on the one-dimensional system of figure 3.7. The state equation for the velocity of the block in this model is represented by:

$$\dot{x} = f(x) = \begin{bmatrix} \dot{x} \\ -\frac{k}{m}x + \frac{F}{m} \end{bmatrix} \tag{3.6}$$

The belt is running at a constant velocity $v_{dr}$, and the force $F$ is limited by the maximum static friction force. The relative velocity of the block is $v_{rel} = \dot{x} - v_{dr}$. At static phase, the block relative velocity is equal to zero. The external force increases since the force inside of the spring increases as it is extended. When the maximum static force is reached, the block will slip and the external force is reduced.

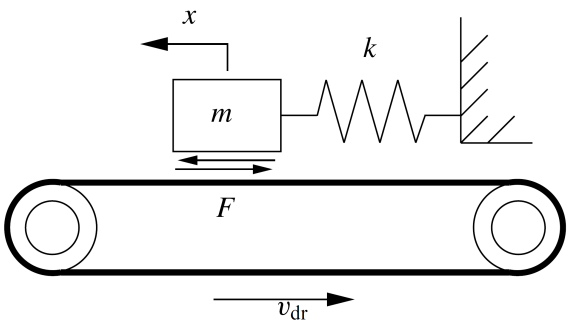


Figure 3.7: 1-DOF model with dry friction

### 3.1.2. Friction models

The possible friction models are presented that include the stick-slip phenomenon. This was thoroughly discussed in Huisman Equipment [11]. For our understanding the following friction models are shortly addressed: Coulomb, Viscous, combined Coulomb-Viscous and the Stribeck friction model as described by Andersson et al. [1].

*Coulomb friction model*

$$F_c = \mu \cdot N \tag{3.7}$$

Here $\mu$ is the coefficient of friction and N is the normal force acting on the contact surface. The coulomb friction force is often simplified as: $F = F_c sign(v)$. This causes trouble in simulations since the sign function will change frequently at zero velocity.

*Viscous friction model*

For model simulations mostly the coulomb friction model turns out to be non-linear. To solve this problem, a viscous friction model is used which is a lot easier to simulate.

$$F = k_v * v \tag{3.8}$$

Here v is the sliding speed and $k_v$ the sliding coefficient.

*Combined Coulomb and viscous friction model*

$$F = \begin{cases} F_c min(k_{sat}, 1) & \text{if v>0} \\ F_c max(k_{sat}, -1) & \text{if v<0} \end{cases}$$

Here the friction force around zero velocity is made smooth and will continue the be 1 or -1 after the coefficient value $k_{sat}$ is reached.

*Stribeck friction model*

To simulate the effect of the difference between the dynamic and static friction the Stribeck model is used. This model also includes a difference in friction force that will depend on the sliding speed.

$$F = (F_c + (F_s - F_c)e^{(\frac{-|v|}{v_s})^i}))sign(v) + k_v v \tag{3.10}$$

Here F is the friction force, v the sliding speed, $F_c$ the Coulomb sliding friction force, $F_s$ the maximum static friction force, $v_s$ the sliding speed coefficient, $k_v$ the viscous friction coefficient and i an exponent.

The Stribeck friction model has the same disadvantages as the Coulomb model, it is highly non-linear around zero velocity and therefore difficult for simulations.

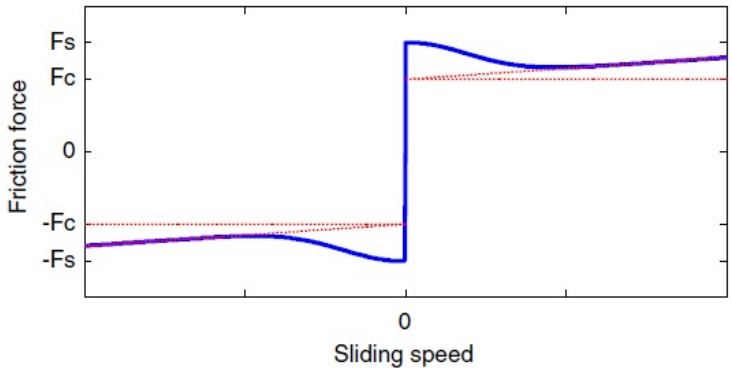


Figure 3.8: Stribeck friction model

The Stribeck force formula 3.10 can be re-written for the friction coefficient $\mu$ as follows:

$$\mu = \frac{F_f}{F_N} = (\mu_0 + \mu_c \cdot e^{(\frac{-|v|}{v_s})^i}) \cdot sign(v) + k_v \cdot v \tag{3.11}$$

The peak tension forces have a height of approximately $900kN$. From earlier operations with the sawing wire discussed in Tricolore [18], the friction coefficient was measured to be 0.886 at 0.85 m/s. The slope of the friction coefficient at higher speeds is 0.2 was measured to be 0.2. This is similar to the measured friction coefficient in the Baltic ace sawing operation.

The static friction coefficient is calculated in equation 3.12. As an example, the approximate wire angle of 25 degrees, a stick friction force of $900kN$ (average peak height) and holding tension of $300kN$ is used to get the static friction coefficient.

$$\mu_s = \frac{F_f}{F_N} = \frac{cos(25) * (900 - 300))}{sin(25) * (900 - 300)} = 1.080(atv = 0) \tag{3.12}$$

Finally, the static and dynamic friction coefficients are substituted into formula 3.11, this results in the graph for the friction coefficient shown in figure 3.9.

This resulting tension graph is shown in figure 3.10, which is acquired with the following formula, with F2 as the holding tension of $300kN$. The Stribeck friction model is close to reality and therefore it is used in the simulation model, which is later discussed in chapter 4.

$$F_1 = F_2 \frac{1 + \mu \cdot tan(\theta)}{1 - \mu \cdot tan(\theta)} \tag{3.13}$$

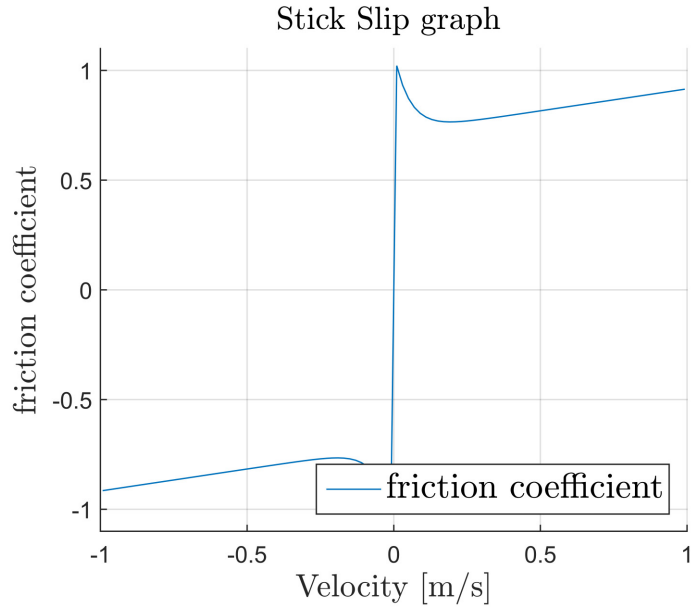


Figure 3.9: Friction coefficient

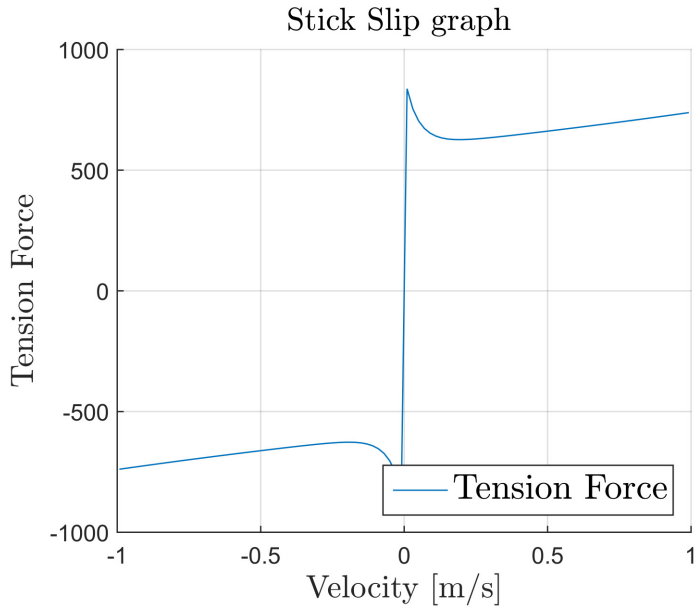


Figure 3.10: Stick-Slip tension

## 3.2. Abrasive Friction and Wear

It is obvious that in the sawing operation the wreck needs to be cut with the sawing wire. The plastic deformation at the surface of the wreck is made thanks to the harder material of the sawing bushes. Generally, the cutting material needs to be 10 – 30% harder than the softer material to generate a ploughing or grooving action as specified by Straffelini [17]. The abrasive friction adds an extra abrasive friction coefficient $\mu_{abr}$ to the friction coefficient. In general, the friction coefficient can be divided into two parts, the adhesive part between the two sliding bodies and the abrasive part. The total friction coefficient is the sum of these two: $\mu = \mu_{ad} + \mu_{abr}$. Little is known about the abrasive contribution to the friction coefficient concerning the sawing wire operations. The angle of attack and the difference in hardness of the material should be taken into account for this calculation. Depending on the angle of attack of the bush-surface, the abrasive coefficient $\mu_{abr}$ can range from 0.05 to 0.37. The total friction coefficient was measured in the sawing operation, therefore the abrasive coefficient $\mu_{abr}$ is not researched further.

## 3.3. Inertia

The other phenomenon that could cause for a similar peak in the tension is considered to be the inertia of the sawing wire. The weight of the sawing wire is around $3.62Te$ , adopted from Huisman Equipment [11]. This is rather small for the forces acting on the wire. The pulling winch is around $70Te$ and the holding winch around $30Te$, adopted from Boskalis [3]. Therefore the weight of the wire is less than 10% of the forces acting on it. Also considering the low acceleration of the winch of $0.2m/s^2$ it is reasonable to assume that the inertia does not cause such a large peak in the tension as measurements show. Though it might be of influence when the acceleration is increased.

## 3.4. Heave Compensator

The heave compensator cylinder compensates the vertical movements of the barges so that the tension force in the sawing wire is not affected by its movement. The vertical movement can be translated to an extension of the saw wire by taking into account the angle of the sawing wire leaving the barge. The vertical velocity is multiplied by the sine of this angle resulting in the necessary compensation length. In figure 3.11a this situation is shown in a simple overview. The set-up of the heave compensation cylinder is shown in figure 3.11b.

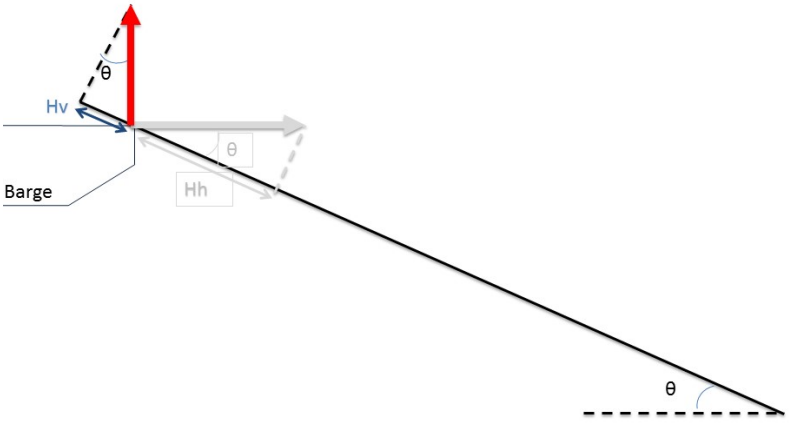


(a) Heave motion barge

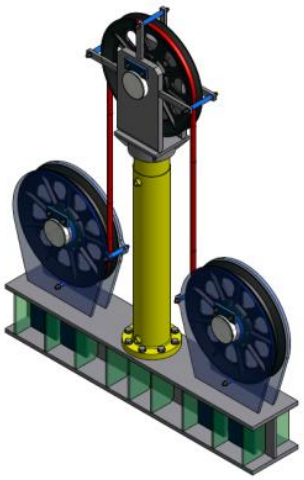

(b) Heave compensator cylinder from Boskalis [4]

Figure 3.11: Heave compensator set-up

## 3.5. Conclusions

The peak tension seen in the graphs of the measurements is caused by the difference in the static and kinetic friction coefficients, this is called the breakaway force. This breakaway force generally 20 – 30% higher compared to the constant tension part. When the velocity of the winch is compared with the tension it is clear that the tension peak takes place before the sawing wire is moving. Secondly, the stick-slip friction is taken into account in the sawing wire simulation by use of the Stribeck friction model. The stick-slip phenomenon occurs when the velocity of the wire falls back and the friction coefficient comes close to the static friction coefficient. This causes for intermittent movement of the sawing wire. The sawing wire inertia is considered not to play a significant part in the creation of the peak tension in the beginning of the sawing cut. Furthermore, the heave compensator measures the heave motion at the fairlead position of the barge and multiplies this with the sine of the sawing wire angle. The information is then used to increase or decrease the stroke of the cylinder. This will lower the tension in the sawing wire that is otherwise experienced due to the heave motions of the barge.

# 4

# Model

The model that is made in Orcaflex can be explained by figure 4.1. The wreck is shown here as a blue shape that is modeled as a round cylinder. From pictures taken during the operation is seemed reasonable to assume the round shape of the wreck. The highest forces will be located at the corners and therefore these will be rounded in an early stage as shown in the test setup in figure 4.2. The sawing wire in yellow is modeled as small elements, with a comparable size as the bush-length. When this line comes in contact with the blue shape, the normal force is multiplied by a friction constant to generate a friction force. This friction force works in opposite direction compared to the movement of the wire. The model is explained in detail in this chapter.

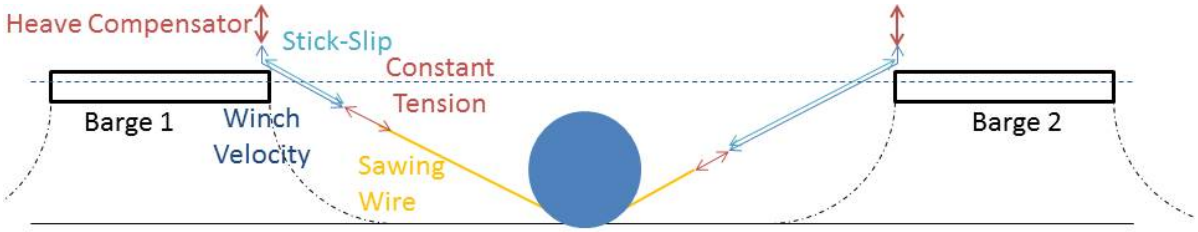


Figure 4.1: Overview of the model

Figure 4.2: Rounding of the corners

## 4.1. Barges

For the simulation of the barge motions in Orcaflex the RAO's (Response Amplitude Operator) as explained by Journée and Massie [12] needed to be calculated beforehand. The calculation of the RAO's has been performed in the program AQWA, which produces a sheet of response forces for incoming waves. The models of the barges that are given as input for AQWA were based on Veritas [21] and Mammoet Salvage [13]. The resulting RAO's were compared with the RAO's that are provided for the Stemat barge in Morphett et al. [14]. The RAO's were found to be similar to the provided document and are considered to be correct. The complete RAO results can be seen in Appendix D.

The RAO's and QTF's were generated with the use of the hydrodynamic diffraction analysis. Since only the diffraction is used, the model was made with submerged elements only. The geometry of the barges can be seen in table 4.1.

| **Specifications Stemat 89** | |
|---|---|
| Draught | 3m |
| Displacement weight | 7604 Te |
| Length | 80m |
| Breadth | 24m |
| Depth | 5 m |
| Kxx | 9m |
| Kyy | 23.6m |
| Kzz | 24.24m |

(a) Specifications Stemat 89

| **Specifications Mammoet MSB3301** | |
|---|---|
| Draught | 3m |
| Displacement weight | 7815 Te |
| Length | 100.5m |
| Breadth | 30.5m |
| Depth | 6.1 m |
| Kxx | 9m |
| Kyy | 25.3m |
| Kzz | 27.02m |

(b) Specifications MSB3301

Table 4.1: Geometry of the barges

Six wave directions were used for the calculations in AQWA. The range of directions was -180 to 180 degrees with a 30-degree interval between directions. Wave frequencies ranged from 0.025 Hz to 0.333 Hz with an element mesh size generated according to the frequencies in the range of interest.

Resulting RAO for the Stemat barge in surge motions is seen in in figure 4.3, where the dent in the beginning of the graph shows an error because the graphs should show a smooth decay. This error is due to a numerical instability on the 3D diffraction tools of irregular frequencies discussed in chapter 7-45 of Offshore Hydromechanics by Journée and Massie [12]. To correct this error, the graph is smoothed.

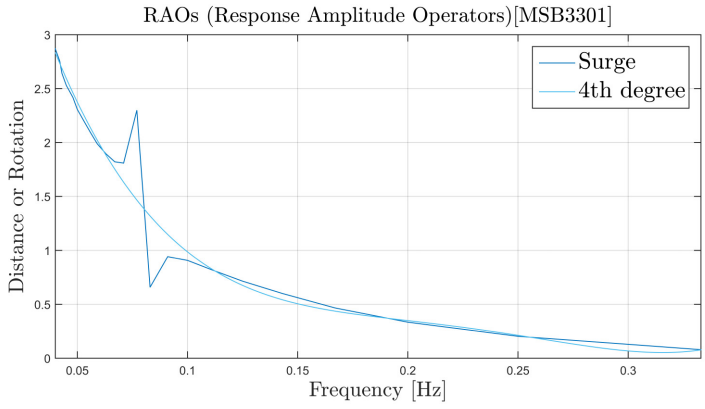


Figure 4.3: RAO Stemat barge

In general, there are two type of RAO's that can be used for simulation: wave load RAO's ór motion RAO's. The motion RAO's are used when the external forces working on the vessel are relatively low. High forces can be lifting of an object or in our case the sawing of a wreck with high tension on the sawing wire. Therefore the barge responses are inserted into Orcaflex as wave load RAO's, though they show similar results in the model.

The set up of the mooring lines is based on the mooring report of Boskalis and Mammoet Salvage [5] and their influence to the barge motions is later calculated by Orcaflex.

## 4.2. Sawing wire

As shown in figure 4.4 the sawing wire consist of a long steel wire with bushes slided onto the wire. Before the sawing operation, the steel wire is drilled underneath the wreck and the bushes are placed on the wire. When the wire is almost filled with the bushes, the steel wire is extended under tension. When the wire is extended extra bushes are placed with tightening bolts on the end. When the tension is released the bushes will be packed closely together. This so-called pre-tension on the sawing wire is around $70Te$.

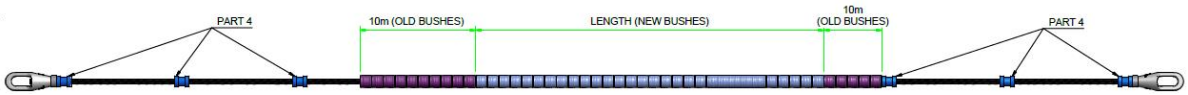


Figure 4.4: Sawing wire assembly

In the Orcaflex model, the sawing wire is included as a line with a diameter and stiffness similar to the wire that was used in the sawing operation. Though the bending stiffness was not included into the model since it is difficult to know how much pre-tension is still present in the wire when the tension winches are pulling it through the wreck.

The length of the sawing wire used in the model is $85[m]$, while maintaining the total mass of the submerged weight of $3.62[Te]$. The weight per meter inserted into the Orcaflex model is then $0.04[Te/m]$. The length between nodes in the model is taken similar to the bush length of the sawing wire $0.112[m]$, as indicated in figure 4.5.

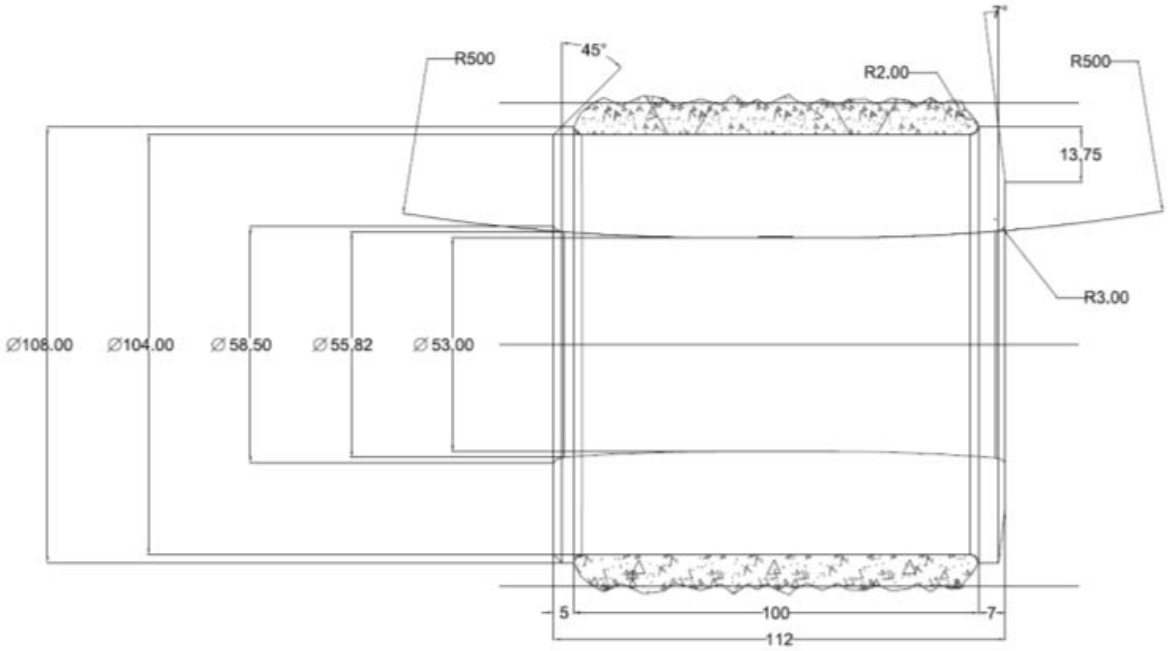


Figure 4.5: Bush dimensions

## 4.3. Friction model

The friction is modeled in two parts. There is a constant friction present in the cylinder shape that represents the wreck in the model, this shape is shown in figure 4.6a. The diameter is 30$[m]$ to represent the average contact length between the wire and the wreck. The constant friction part is modeled as a friction coefficient and works as a Coulomb friction as described in chapter 3. If a node of the sawing wire comes in contact with the shape it will use the specified friction coefficient to create a friction force depending on the normal force experienced. As shown in the constant tension in figure 4.6b the mean normal force experienced over the range of the sawing wire that comes in contact with the shape is around $10kN$. The high case is not of interest at the moment. The mean constant friction force created by the friction of the shape is approximated by:

$$F_f = \mu \cdot F_N \cdot Length = 0.8 \cdot 10[kN/m] \cdot 30[m] = 240kN \tag{4.1}$$

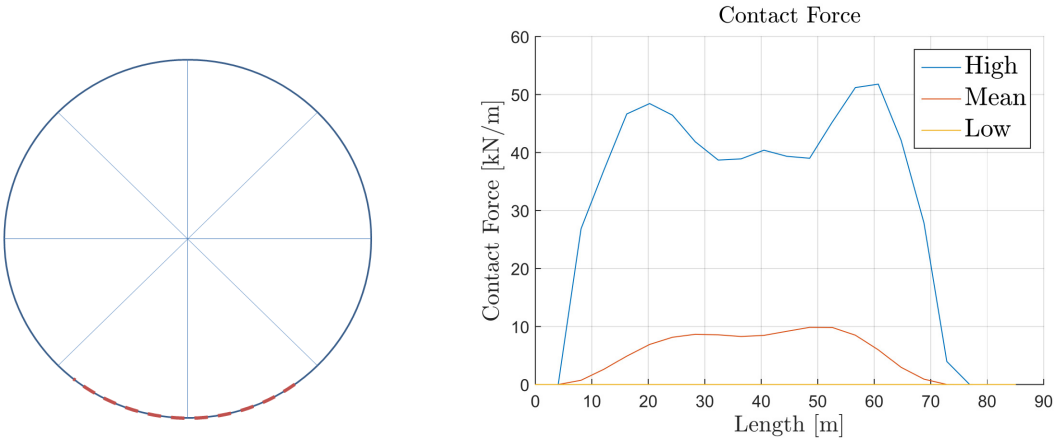


(a) Contact friction

(b) Contact force

Figure 4.6: Friction shape

The other part, the Stick-Slip friction, is covered by adding a damper to both sides of the sawing wire that include the change from the static to the dynamic coefficient of friction by applying a higher tension on the wire when the velocity is close to zero. Because the constant part of the friction is already covered by the shape this part is subtracted from the influence of the damper. The stiffness of the damper is set to zero so that it does not imply extra tension when it is elongated or compressed. As discussed before in chapter 3 the Stribeck model is unstable for zero velocity in simulations. Therefore the dampers on both sides are equal and have an opposite working tension at zero velocity, this makes the model stable at static simulation but loses its peak tension. In figure 4.7 the tension is shown as a reaction to different velocities. The solution for the peak tension will be discussed next.

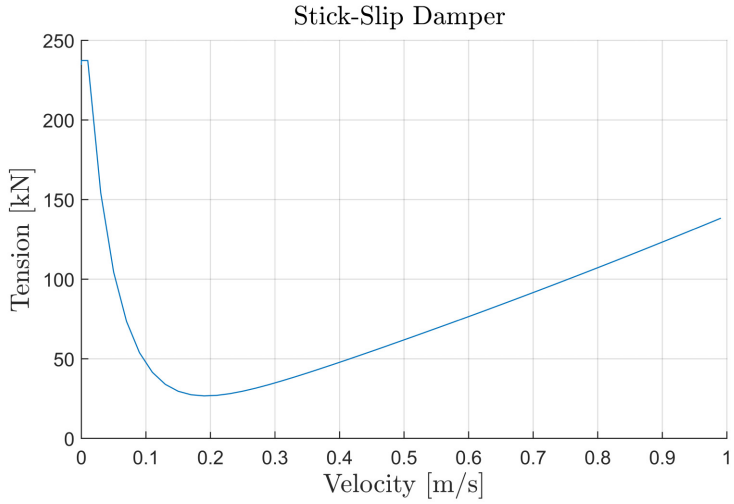


Figure 4.7: Stick-Slip Damper

## 4.4. Winch set-up

Winch settings for the right winch are shown in tables of Appendix A. The resulting tension and velocity settings are shown in figure 4.8. It should be pointed out that the tensioner shown here gives a short extra tension on the sawing wire that represents the breakaway force needed to get the sawing wire in motion. The value of the breakaway force is approximated by taking a $20-30\%$ extra of above of the average tension force as was described in chapter 3. The value of the peaks shown in the figure below is $258kN$, which is the calculated difference between stick and slip friction forces for a friction coefficient of 1.1 for sticking and 0.8 for slipping.

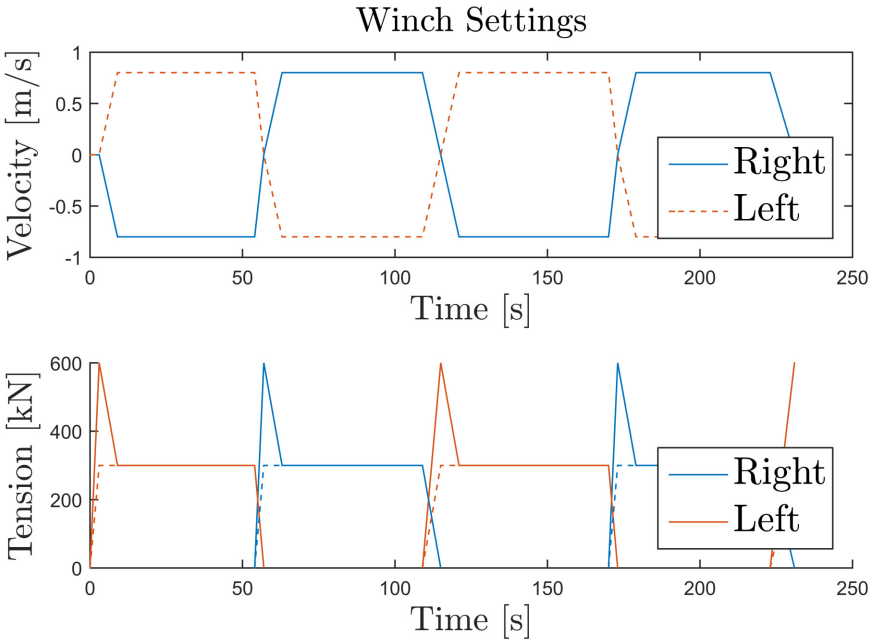


Figure 4.8: Winch setting

The winch settings are designed so that both the winches work exactly opposite and change from master to slave to change direction. The master winch is in haul-in phase and has a velocity setpoint of 0.8 m/s. At the same time the slave winch is paying out wire, during pay-out the winch has a holding tension of $300kN$ so that there is enough force to cut the wreck with the sawing-wire. The time display of the various stages in the

table of Appendix A is set up such that the comparison with the measurements will give a clear picture. This way we can see how much the model relates to the real case. To be more specific, the stage duration is chosen similar to the measurement constant-tension values. To give an indication of this constant tension the set point is shown in figure 4.9. In this graph, the measured velocity of both winches is shown together with the setting for constant tension. When the value is equal to 1 the constant tension is active.

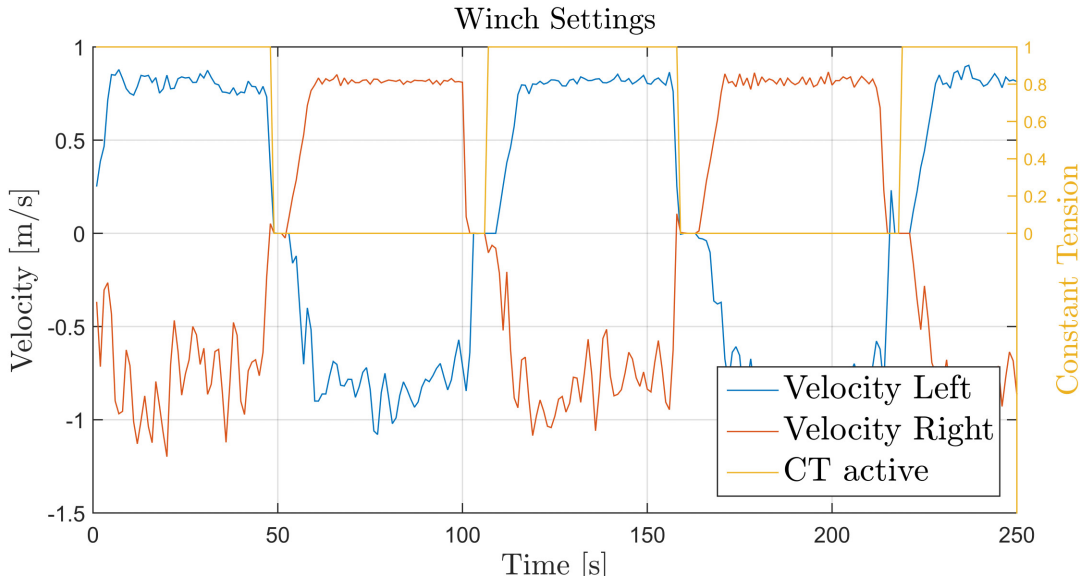


Figure 4.9: Constant tension

## 4.5. Heave compensator

The heave compensator is modeled as a winch in Orcaflex. The winch is velocity controlled to compensate the heave motion of the barge just like it did in the salvage operations. The velocity set-point is operated through a code in python, this code can be seen in appendix B. The velocity of the barge at the fairlead position is measured by the script and multiplied by the sine of the sawing wire angle, just as described in chapter 3.

The fairlead velocity could not directly be measured in the simulation program Orcaflex, though the angular velocity of the barge around its axis could be measured. As shown in formula 4.2 the angular velocity around the y-axis is multiplied by the arm measured from the center to the fairlead position as shown in figure 4.10. Table 4.2 shows the variables that are sent to the python script every time-step.

$$V = \omega \cdot r \tag{4.2}$$

| # Details of the things to be controlled: | |
|---|---|
| ControlledObject | Barge left |
| ControlledVariable | y-Angular Velocity |
| ControlledObject 1 | Barge left |
| ControlledVariable2 | x-Angular Velocity |
| ControlledObject3 | Winch Tension Left |
| ControlledVariable3 | Declination |
| ControlStartTime | 0 # simulation time controller becomes active |

Table 4.2: Settings Heave Compensator

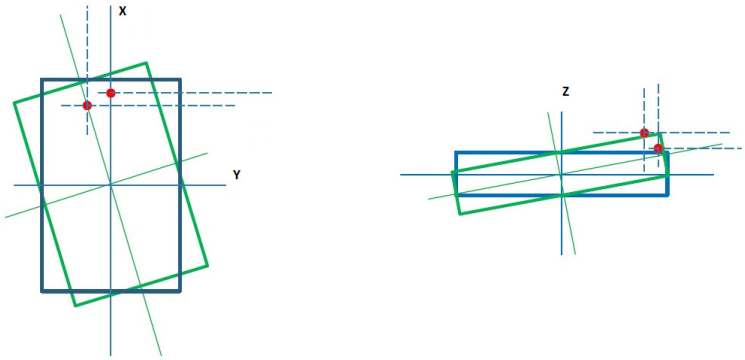


Figure 4.10: Influence pitch and yaw

## 4.6. Environmental input data

Generally, the measurement graphs that are shown in this thesis report are of the sixth cut in a range from 46420 to 47734 seconds. This was used since it has a continues signal. The average significant waves height measured during this interval is $h_s = 1.26[m]$. The average wave period over this time interval is $t_s = 4.09[s]$. These values were used as an input value for the modeling of the sawing operation. The wave direction was not clearly measured and therefore 3 directions were taken to mimic the actual case. The signal of $H_s$, $T_s$ and Tide are given for the complete range of the sixth cut in figure 4.11.

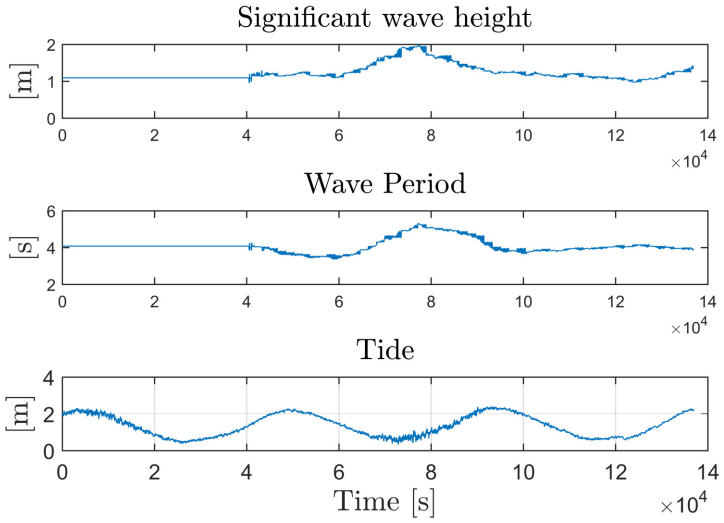


Figure 4.11: Environmental Measurements

The wave train that is included into the model is based on 3 wave directions and a JONSWAP frequency spectrum. The JONSWAP spectrum is a typical wave frequency spectrum for the North sea location based on extensive measurements described by Holthuijsen [10]. The spectrum is seen in figure 4.12. The directional spectrum that is used in the model is shown in figure 4.13.

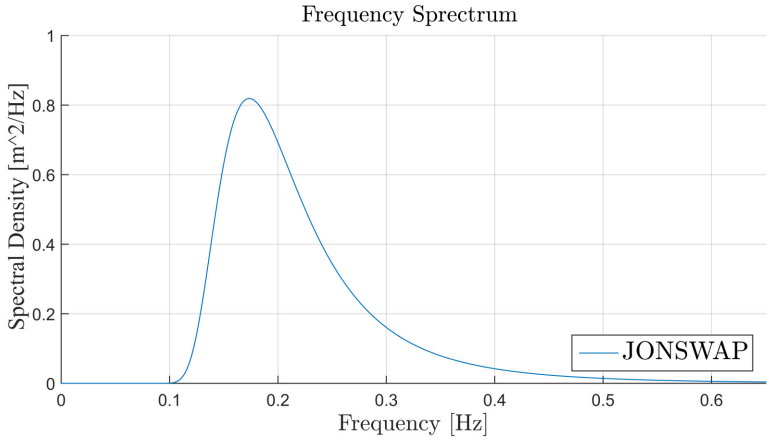


Figure 4.12: Frequency spectrum

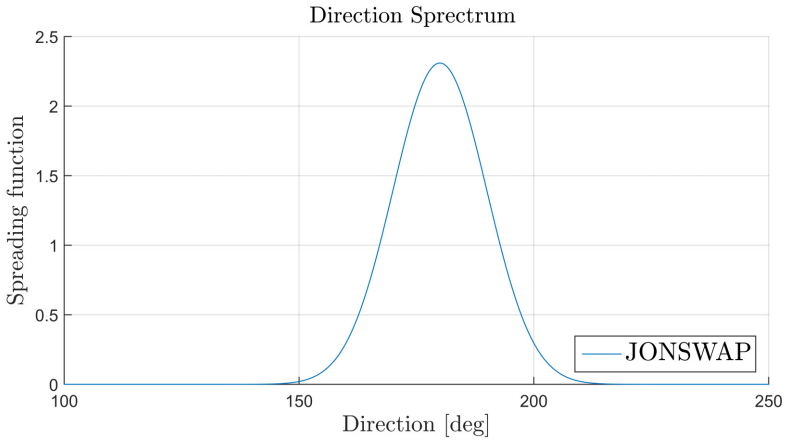


Figure 4.13: Direction Spectrum

## 4.7. Simulation Results

Finally, simulations were performed with the complete model including the velocity winches, tension winches, solid friction, stick-slip friction, barge movement and heave compensator. First, the resulting tension and velocity of the winches is shown in time domain. Following these results is the frequency domain result of the tension in the winch. In chapter 5 these results are compared with the measurements that were taken during the sawing operation.

### Time Domain

The tension of both winches is an important measure for the operation. The simulation resulting from the right tension winch is shown in figure 4.14. One sawing cycle of the sawing wire going from left to right takes approximately 50 seconds, so in this result the sawing wire goes back and forth two times. The difference in holding and pulling tension is clearly seen at $700kN$ when the winch is pulling and $375kN$ when the winch is paying out. Further things to notice in this graph is the peak tension in the beginning of the sawing cycle. The peak is caused by the breakaway force as discussed earlier.

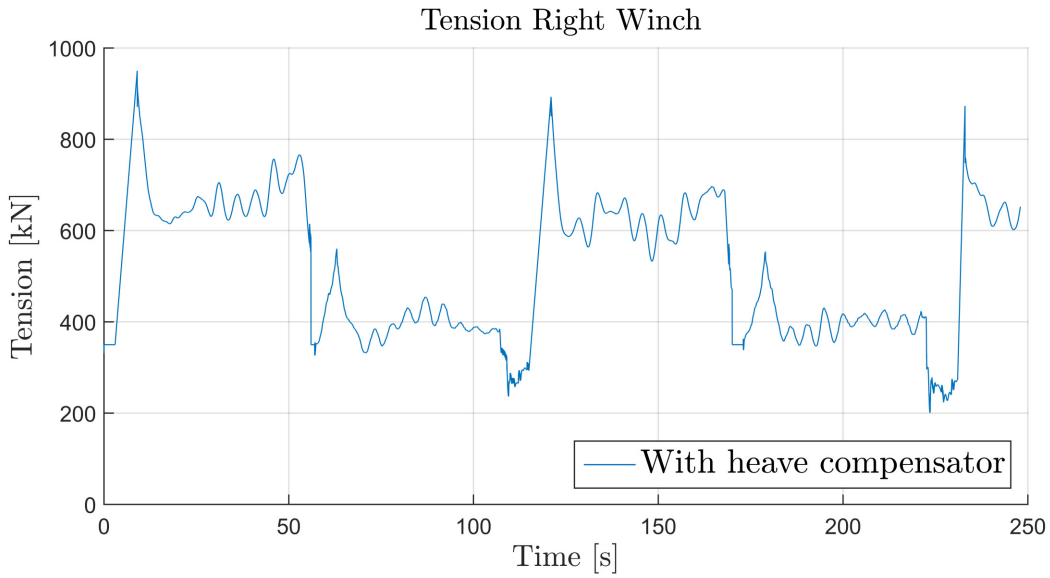


Figure 4.14: Tension of right winch

The velocity graph for the same winch is shown in figure 4.15. The negative velocity of the first 50 seconds represents the pulling-in of the sawing wire. The setpoint of the velocity for pulling in is reached perfectly, this does not represent the reality correctly but was a limiting factor of the simulation program Orcaflex. When the winch pays out wire it is set to keep a constant tension on the wire, therefore it is more irregular for the second 50 seconds in the graph. Furthermore, it is clearly seen that the winches stop moving for a couple of seconds when the sawing wire reaches the opposite side.

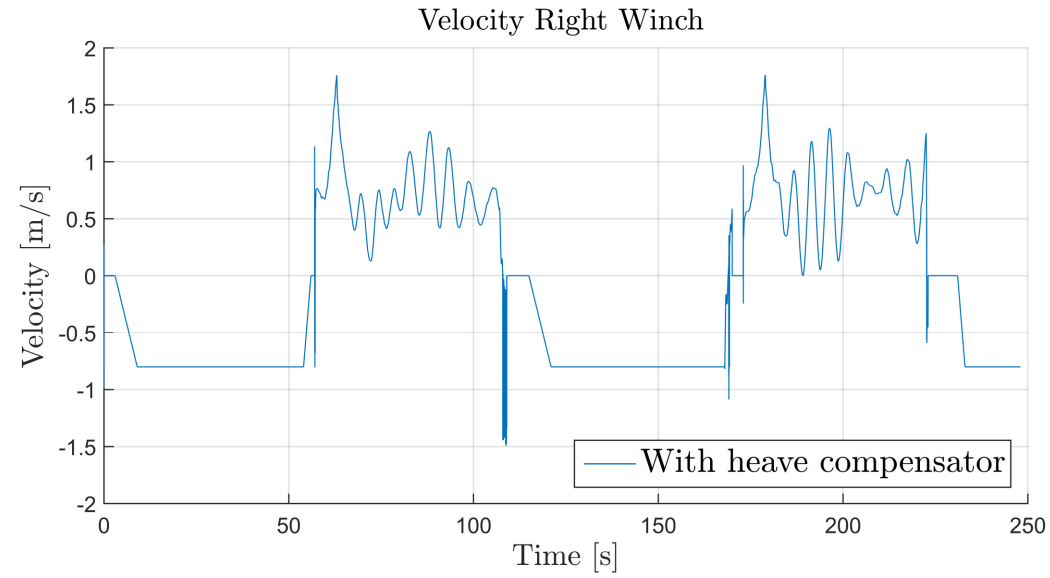


Figure 4.15: Velocity of right winch

### Frequency domain results

The Result of a frequency domain analysis of the tension in the wire is shown in figure 4.16. The resulting peaks represent the energy, measured by the number of times that the peaks in the tension result re-appear. Therefore the higher the peak the more peaks were present at the same frequency. The construction of the frequency domain plot is already discussed in chapter 2.

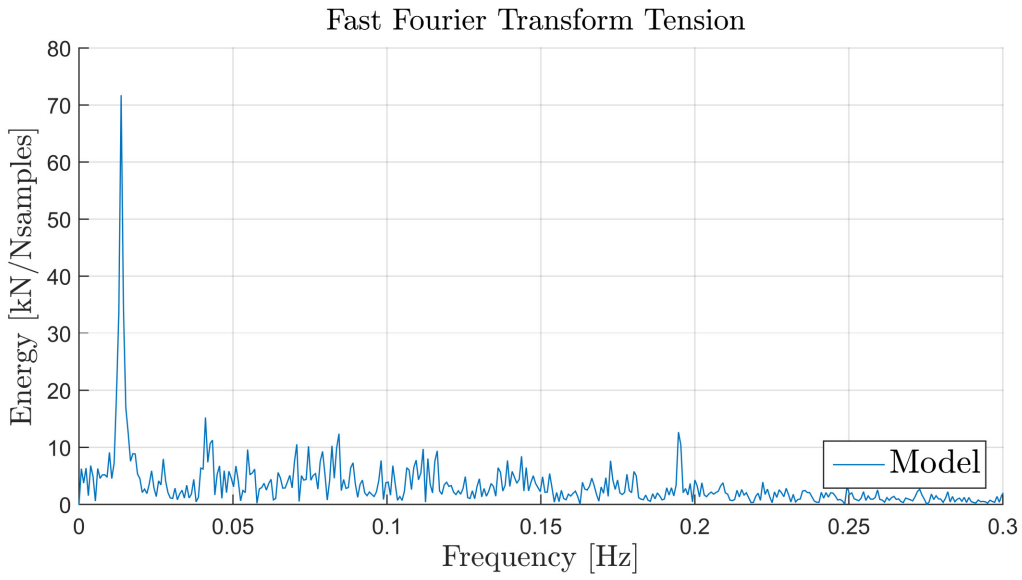


Figure 4.16: Tension of right winch

## 4.8. Conclusions

The simulation model of the sawing wire system has been made in the program Orcaflex. The barge motions are included via force RAO's which were constructed in the program AQWA. The sawing wire was made with small elements representing the bushes. The weight of the complete sawing wire of 3.62[$Te$] was inserted into the model but the bending stiffness was left out. Leaving out the bending stiffness was done because of the high loads of the winches, therefore it was not certain if and how much pre-tension was still present in the wire. The friction in the wreck is covered by a shape in Orcaflex with a coefficient of friction and an extra damper on both sides of the sawing wire that includes the stick-slip friction. The difference between static and kinetic friction is covered by an extra tension at low velocities. The heave compensator is inserted as a winch on top of the barges. The angular pitch velocity of the barges is measured and together with the declination angle of the sawing wire the required stroke of the winch is calculated. Furthermore, the environmental input of the model is based on a JONSWAP spectrum with wave height and period similar to the actual sawing operation. The simulation results of the model look promising and will be compared with the measurements in the next chapter.

# 5

# Comparing the Results

## 5.1. Time Domain Comparison

The comparison of the model with the actual measurements for tension is shown in figure 5.1. The tension peaks show similarity to the measurements both in their height and frequency of occurrence. The breakaway force at the beginning of the sawing cycle is of a similar height as the measurements. Although the peak is not always present in the measurements because of irregularities described in chapter 2, it is included in the model. Also, the further amplitude of the lower peaks fit around the 600 kN, just like the measurements. The holding tension of 375 kN is also correctly modeled. The main difference with the measurements can be seen in the force fluctuations in payout mode, the amplitude is smaller compared to the measurements. This is probably because the model keeps the holding tension better than in reality.

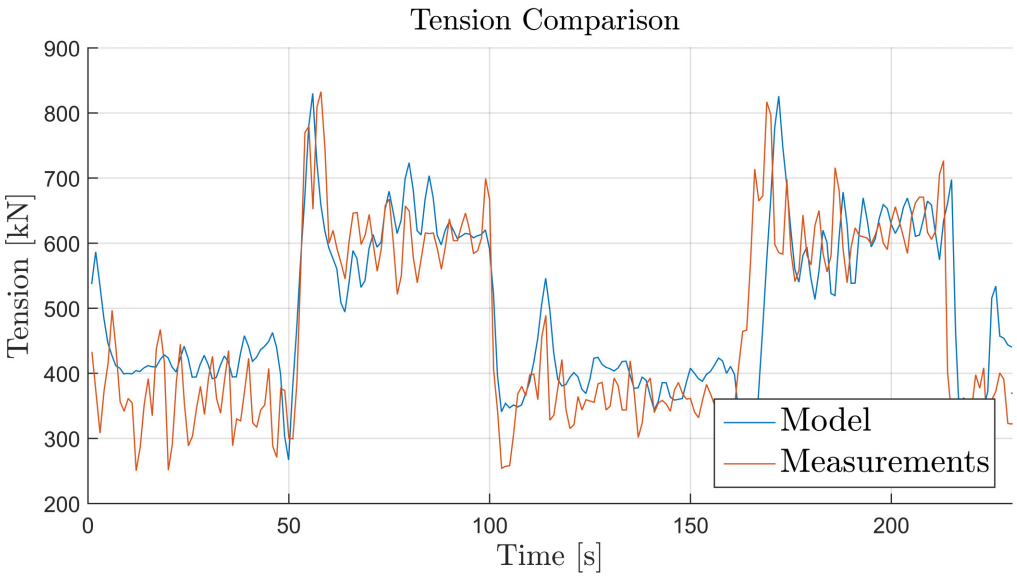


Figure 5.1: Tension comparison

The graph of the velocity comparison is given in figure 5.2, where the model shows a similar result as the measurements. The haul-in velocity is similar and fairly constant. The holding rate is less constant and shows a high frequency of small peaks. The biggest difference between the model and the measurements for velocity can be seen in the overshoot peaks when the haul-in speed is achieved (110 sec.). Furthermore, the paying out velocity of the model has a larger amplitude compared to the measurements. The difference in paying out, both for velocity and tension can be allocated to the limitations of the simulation program regarding the winch. The winch in Orcalfex is very simple and does not include damping or inertia of the drum.

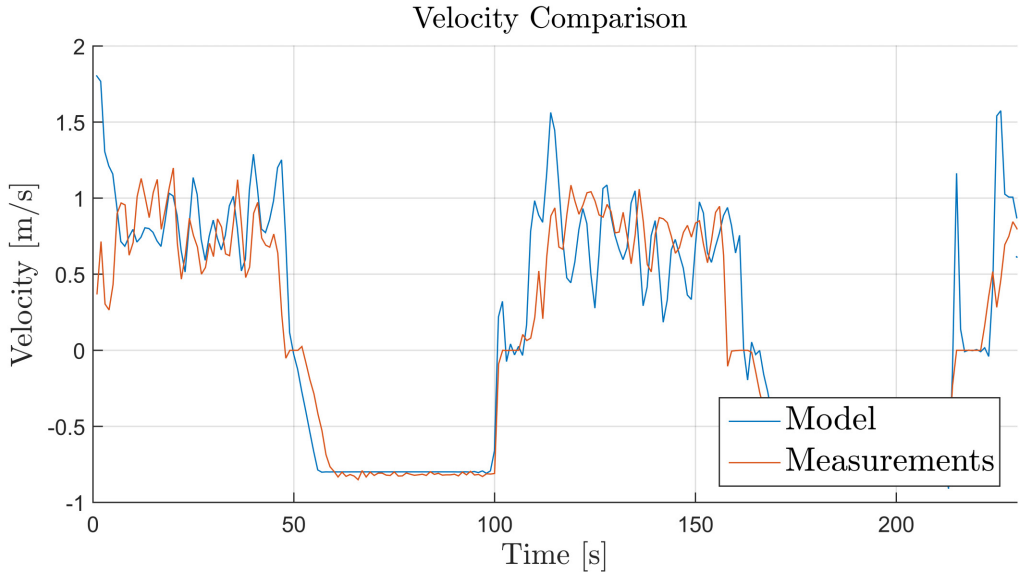


Figure 5.2: Tension comparison

Looking at a longer time-trace of the tension comparison as shown in figure 5.3, it can be seen that there is a run-off between the graphs. Apparently, the sawing stroke in the measurements sometimes has a longer or smaller stroke that of the model. This is not wrong but it makes the error of the model difficult to predict. When the two graphs are subtracted and the mean is taken, the error can be around 25 percent. This is not correct and therefore a frequency domain analysis will be discussed next to compare and validate the model.

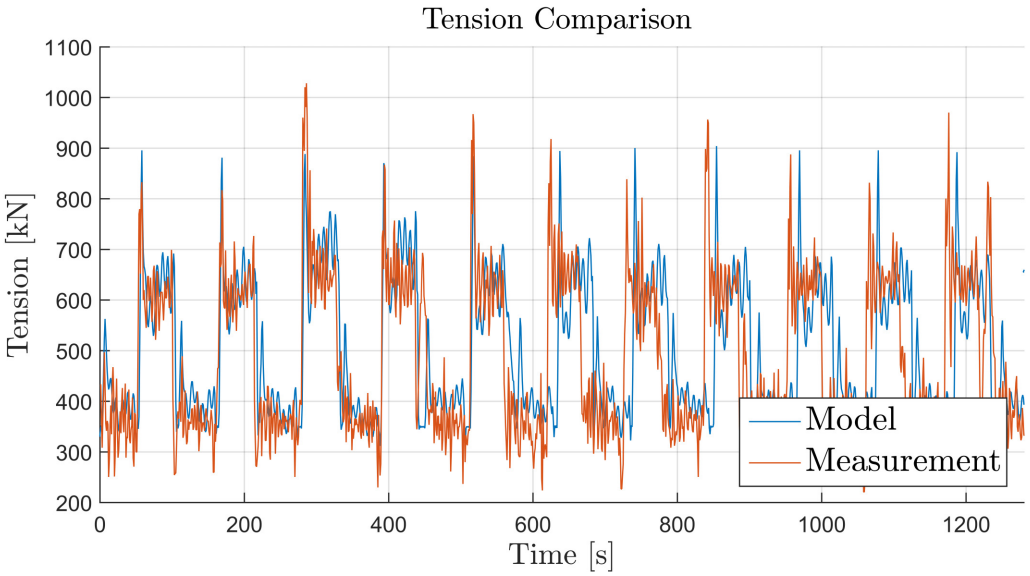


Figure 5.3: Tension comparison

## 5.2. Frequency Domain Comparison

The comparison of the model and the measurements in the frequency domain is shown in figure 5.4. From this graph, it becomes clear that the essential tension peaks are taken into account, especially at lower frequencies. At frequencies surpassing the $0.1 Hz$, the graph of the model shows more peaks than the graph of the measurement. This is also allocated to the limitations of the simulations program Orcaflex.

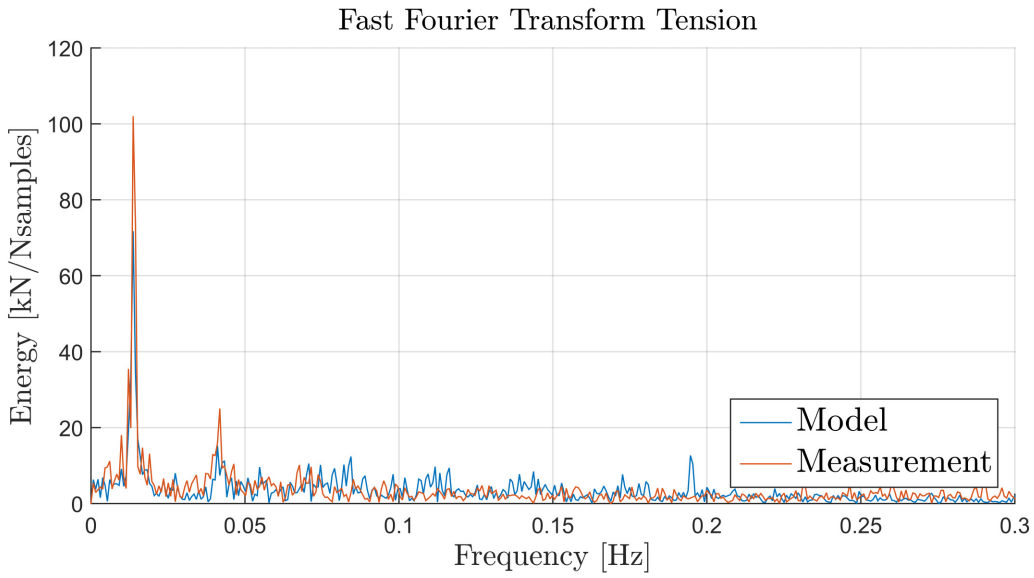


Figure 5.4: Comparison of tension in Frequency domain

## 5.3. Heave Compensator

The effect of the heave compensator that is included in the model can be seen in figures 5.5 and 5.6. Shown in these graphs is the lowered amplitude of the tension, especially in the paying out phase of the sawing procedure. The big peak in the beginning of the sawing motion is not compensated by the heave compensator, since the peak tension is not caused by motions of the barge but due to the friction. Since it is not clear how the tension peak is influenced by the control of the heave compensator, more investigation in the future is necessary.

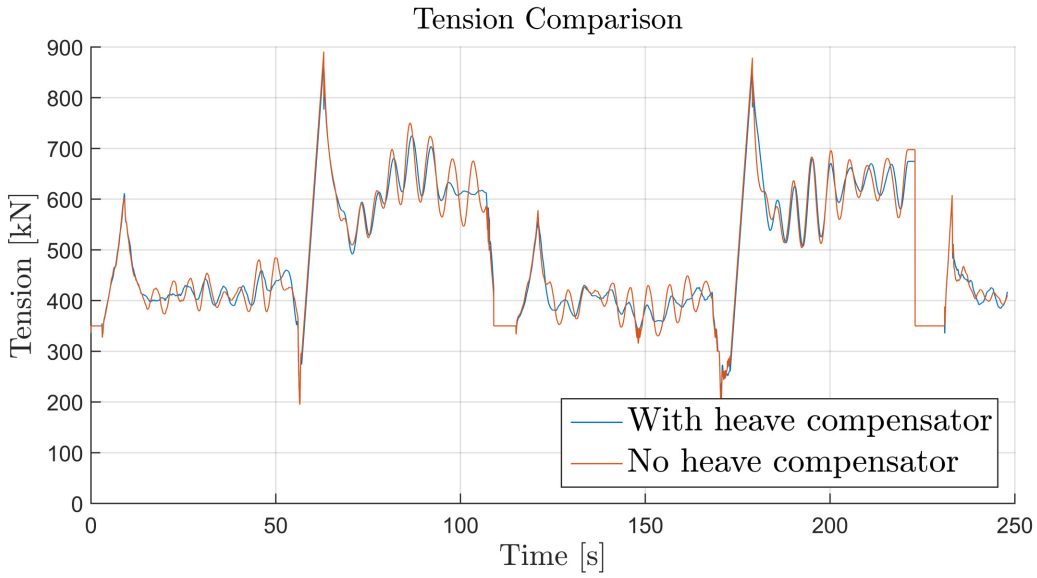


Figure 5.5: Heave compensator effect left

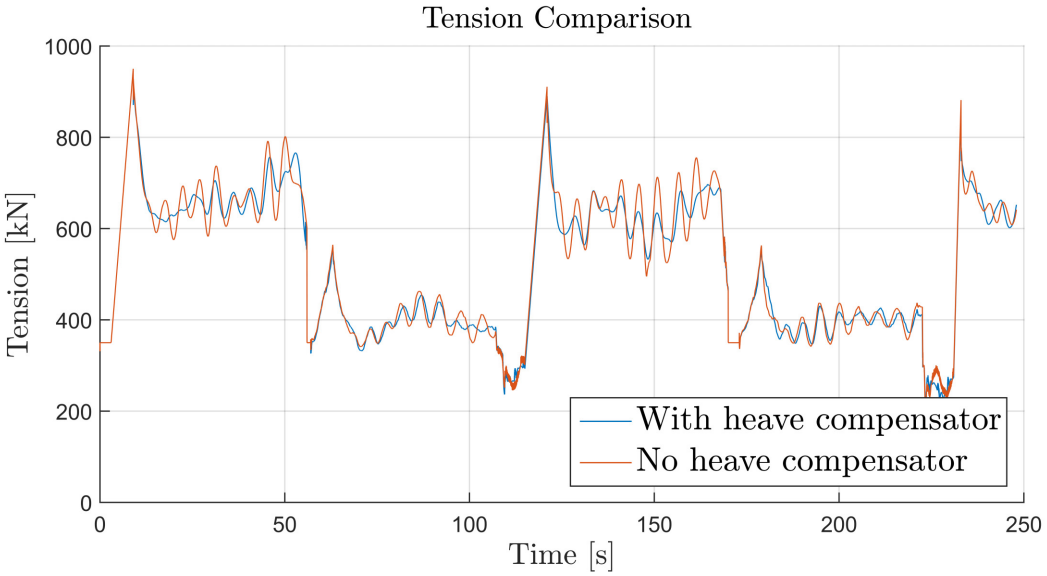


Figure 5.6: Heave compensator effect right

The velocity graphs for the simulations with and without the heave compensator can be seen in figures 5.7 and 5.8. Important to recognize is the difference between the graphs with and without heave compensation, in which the amplitude is sometimes smaller or larger. This is explained by the fact that a positive pitch motion of the barge results in a positive stroke of the heave compensator's cylinder. In order for this stroke to happen, the winch needs to pay out more wire. Therefore, the influence of the heave compensator is only clearly observed in the tension graphs discussed before.

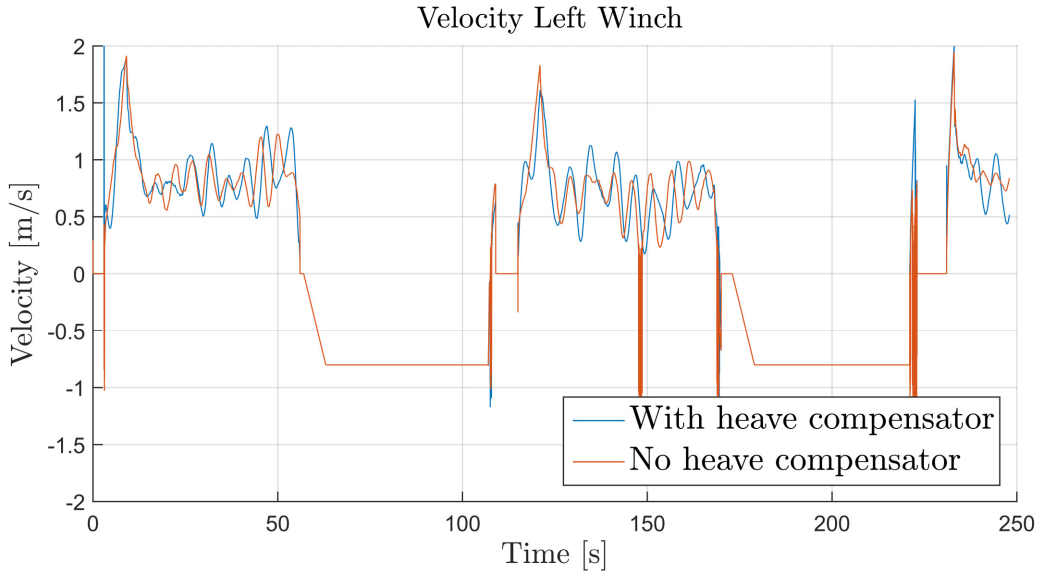


Figure 5.7: Heave compensator effect left

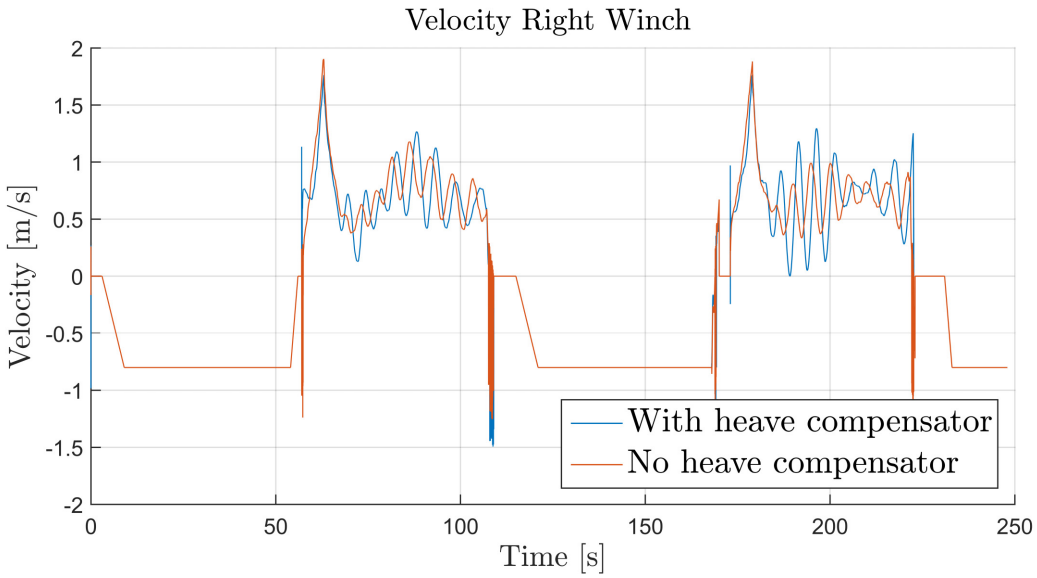


Figure 5.8: Heave compensator effect right

The barge movement in the model is compared to the barge movement in the measurements in figures 5.9 and 5.10. The heave compensator only takes into account the heave motion of the barges. Though in the design assessment it is explained that the surge motion has a large influence on the tension in the sawing wire as well. In figures 5.9 and 5.10 the motions of the model and the measurements are compared, which show similar amplitudes.

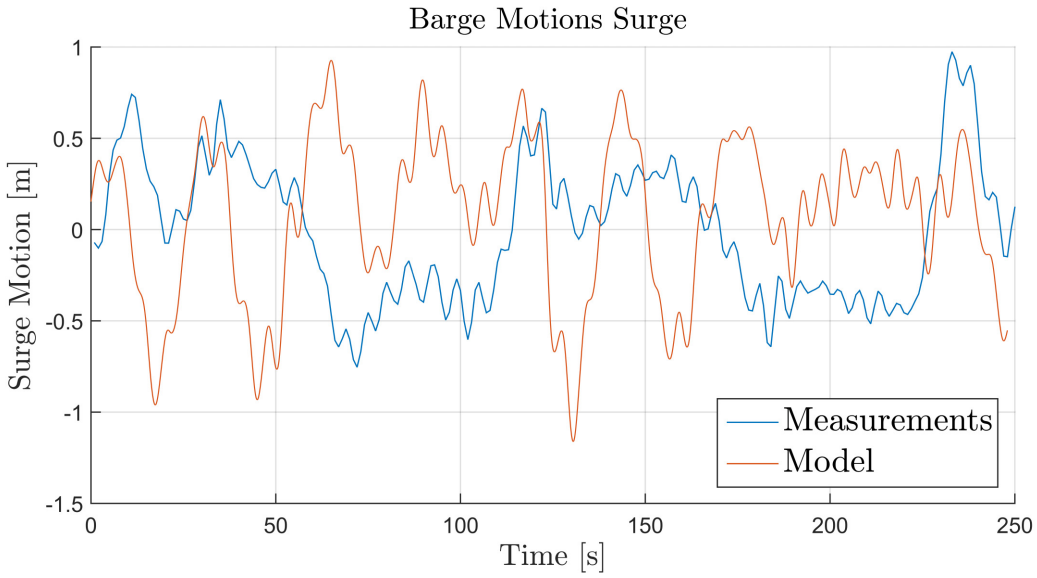


Figure 5.9: Barge Motion in Surge

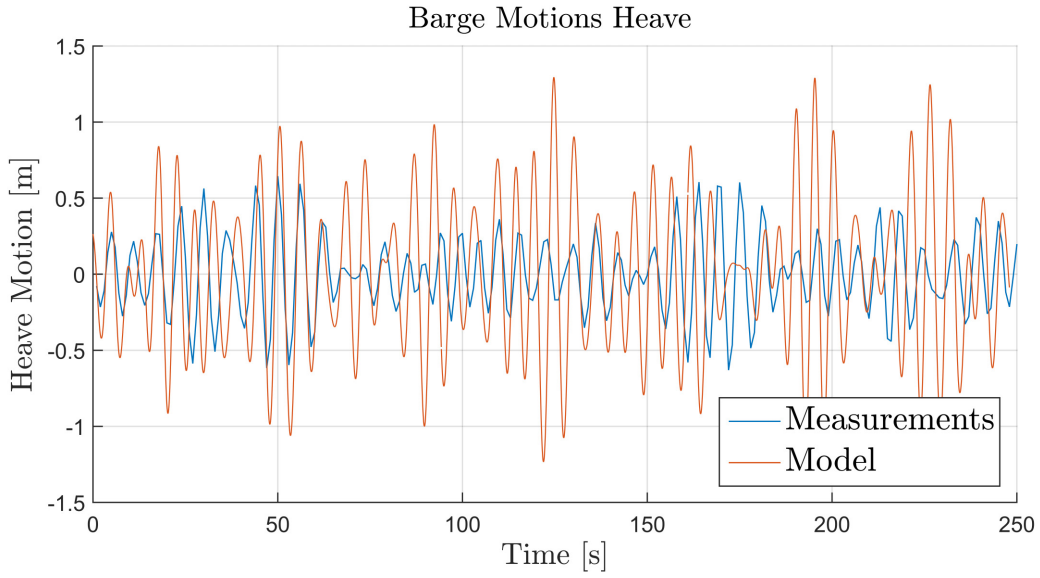


Figure 5.10: Barge Motion in Heave

## 5.4. Conclusions

The tension of the model and the measurements are comparable. The peaks that are shown in a longer time-trace sometimes have higher or lower peaks, but generally do not vary much. The frequency domain comparison of the model and the measurements shows very similar energy peaks in the lower frequencies. The model has some more peaks in the higher frequencies compared to the graph of the measurements. This is possibly due to the limitations of the simulation program used. The heave compensator as modeled in the model shows a reduction of the tension amplitude when it is turned on compared to a model where it is turned off. The breakaway force in the beginning of the sawing cycles is not compensated with the heave compensator since this is not caused by the movement of the barges but by friction. The velocity graph shows that the heave compensator sometimes asks a higher or lower velocity of the winch in order to compensate for the barge motions. The movement of the barges in surge and heave motion is compared and show similar fluctuations, thought the barges of the model are moving somewhat more.

# 6

# Design Assessment

In this chapter the design of the sawing wire system is assessed. The first topic discussed is the accidental load scenarios and the winch settings. Secondly the implementation of the system for future operations is discussed. The assessment for future operations includes: accidental load scenario's, difference in wreck diameter and different materials. Final topics discussed are the elimination or reduction of the peak tension and the effect of the heave compensator.

## 6.1. Accidental load scenario's

The accidental load scenario's are based on the mean breaking force of the sawing wire, MBL = 1893 kN. The worst case scenario is a stop of both winches at the same time as the sawing wire is stuck in the wreck and the heave compensators are turned off. It is not acceptable when the tension in the sawing wire surpasses the MBL, therefore there is a maximum allowable wave height for the sawing operation.

The maximum allowable wave height has been checked before, so the results from this simulation model can be compared with the previous results. These results are shown in table 6.1, with a safety factor of 1.5 these results stay well under the MBL. In the table it can be seen that there is a difference between the hold an new simulations. This difference can be allocated to the change of barges in the actual operation, which were included in the new model.

| **Load Case Tp6** | **Max Tension (kN)** |
|---|---|
| Model OLD Draft 4.76 Hs 1.5 | 1012.72 |
| Model NEW Draft 4.76 Hs 1.5 | 904.88 |
| Model OLD Draft 4.76 Hs 1.1 | 833.55 |
| Model NEW Draft 4.76 Hs 1.5 | 856.87 |

Table 6.1: Accidental load cases

### 6.1.1. Winch settings

The winch settings are checked for the case of failure or sudden events that may damage it or create a dangerous situation. The limits for the winches concern both a maximum velocity and a maximum tension. These limits can not be held at the same time since they require a high amount of power, at the velocity limit the tension can not be kept at the highest load and visa verse.

The velocity of the winch also depends on the wave conditions. The heave compensator is moving up or down to compensate for the barge motions, while constantly increasing or decreasing the winch velocity to make this possible. The winch setpoint together with the added velocity for the heave compensator can result in overriding the maximum velocity. The maximum paying-in velocity of the winch is 2.0256 [rad/s], which is around 1.18 [m/s]. When the maximum velocity is reached the winch is unable to pull-in the sawing wire fast enough, causing the tension to decrease and the wire to slow down.

The holding winch is able to have a maximum paying-out velocity setting but this is not activated in the operation. When the maximum pay-out velocity would be reached, the holding tension will rise and sawing wire would slow down. Therefore it is safer to let the winch override the maximum velocity setting for a short period of time.

For the tension on the winch, the maximum torque is 4.6407e5 [Nm] as stated in Huisman Equipment [11], therefore the maximum tension is around 794 [kN]. In the measurements of the sawing operation, it is clear that the overshoot in tension is sometimes higher than this maximum value. The override of the maximum tension or torque is only possible if enough power is present to sustain the torque and the pulling-in velocity. The pulling-in velocity is therefore not set to its limit.

When changes to the velocity or tension settings are desired these will be dependent on the available power. When the tension is lowered the velocity setpoint may be higher, resulting in faster cutting. Therefore this will result in a trade-off between installed power and cutting speed for the future operations.

| | | | |
|---|---|---|---|
| maxSpeed | maximum speed of drum | 2.0256 | [rad/s] |
| r0 | radius of drum at first layer | 0.584 | [m] |
| maxSpeed | maximum speed of drum | 1.175 | [m/s] |
| torqueMax | maximum torque at drum (full throttle) | 4.6407e5 | [Nm] |

Table 6.2: Winch Settings from Huisman Equipment [11]

The power that is needed for the winch to generate both the required velocity and the required tension for the sawing wire is shown in figure 6.1. The power is calculated with formula 6.1. In the figure, it can be seen that the power graph shows a peak at the same place of the peak tension and the rise of velocity. Therefore lowering or eliminating the peak tension would lead to lower required power in the system. Therefore elimination of the peak tension is recommended for future operations and will be discussed later in this chapter.

$$P = \frac{kg \cdot m^2}{s^3} = kN \cdot \frac{m}{s} = kW \tag{6.1}$$

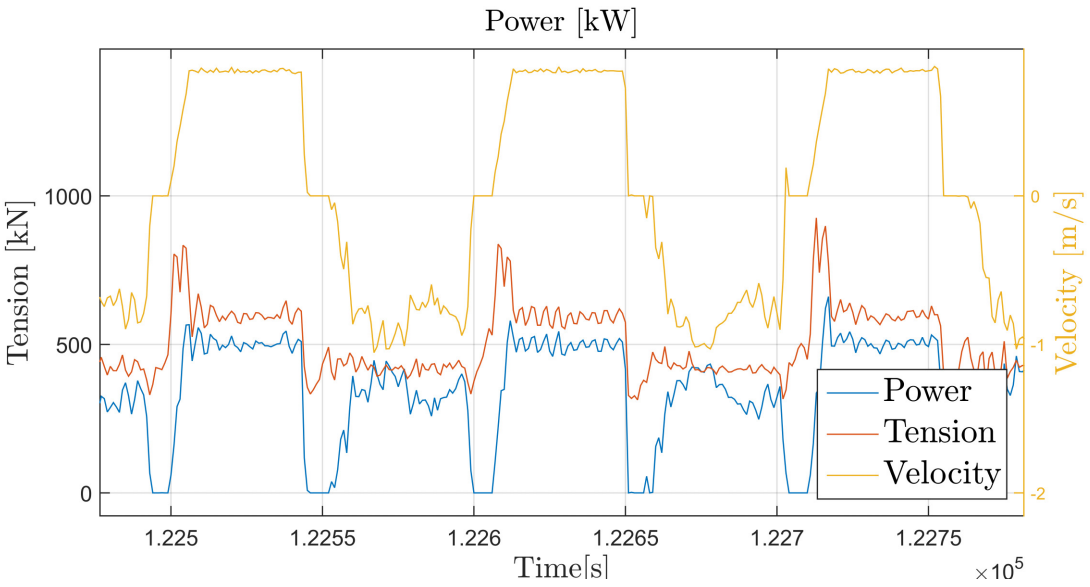


Figure 6.1: Power needed to get both the tension and velocity

## 6.2. Future implementation of the system

For future use of the system, the object that needs to be cut in pieces will be different. Some of the scenarios will include a larger or smaller diameter of the shipwreck or a different material. Some possibilities are shown in figure 6.2 and the implications to the system are discussed shortly.

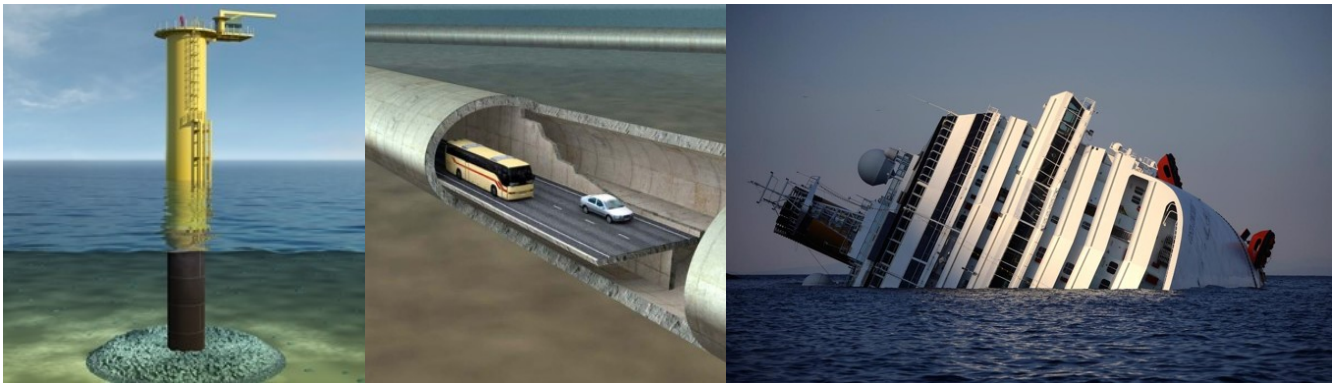

(a) Monopile foundation (b) Concrete submerged tunnel (c) Costa Concordia

Figure 6.2: Some scenarios for next use of the cutting wire system

### 6.2.1. Different diameter - monopile/costa concordia

Future scenarios could include monopile decommissioning in which case the whole system set-up will need to be different, but in general the most important change is the smaller diameter. The friction model for the sawing wire that is discussed in this thesis could still be used but the diameter of the shape in Orcaflex and the coefficient of friction should be changed. The smaller diameter will cause for the pulling forces to decrease which means they will be closer to the holding forces. A bigger diameter will in turn cause for a bigger difference between pulling and holding forces as the contact surface increases. An example of the change of diameter is shown in figure 6.3.

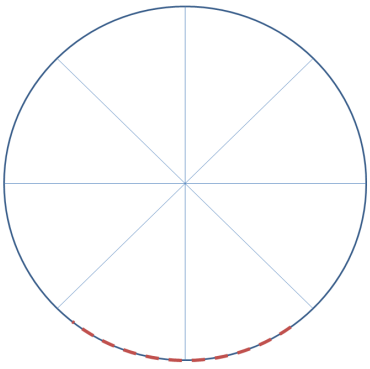

Figure 6.3: Friction block

$$F_f = \mu \cdot F_N \cdot Length = 0.8 \cdot 10[kN/m] \cdot 10[m] = 80kN \tag{6.2}$$

This is the same equation that was stated in chapter 4, but now the contact length of the sawing wire is three times smaller. Because the friction coefficient $\mu$ stays the same for similar material, the required pulling force would be lowered.

### 6.2.2. Different material - tunnel

In the scenario of a submerged concrete tunnel, it is interesting to see how the different material influences the system. The static friction coefficient of steel on concrete or grout is found to be $\mu = 0.57 - 0.70$ Rabbat and Russell [16]. The coefficient of friction is very difficult to predict beforehand since it is not only sliding friction but also abrasive wear of the material. It is advised to do tests of similar material to accurately predict the friction coefficient.

## 6.3. Eliminating The Peak Friction Force

Essentially the peak friction force in the beginning of the sawing cycle is the highest point of interest. The parameters concerning the sawing wire and the applied tension of the winches are influenced by this peak tension. Therefore it is of importance for future operations to decrease this peak. The peak friction force can be eliminated with the use of impulsive control or a lower holding force in the beginning of the sawing cycle.

The lower holding force at the start still generates a lateral forces caused by the friction in the wreck that needs to be overcome. The difference in static friction coefficient and dynamic friction coefficient stays the same, but the total force applied is then lowered with approximately $287kN$. This is the difference between stick and slip friction as calculated in equations 3.4 and 3.5. The normal and lateral forces in the wreck are lowered if the lower holding force at the start is introduced. Let's look at an example:

*The holding force reduced to* $200kN$. *The required pulling force is then only* $700kN$. *The resulting lateral force is* $453.2kN$ *and the normal force is then* $380.4kN$. *Subtracting the weight of the sawing wire of* $3.62Te$ *the normal force results in* $344.8kN$.

After the movement of the sawing wire has started, the tension is increased again to get the required cutting forces. The result with elimination of the breakaway force is shown in figure 6.4.

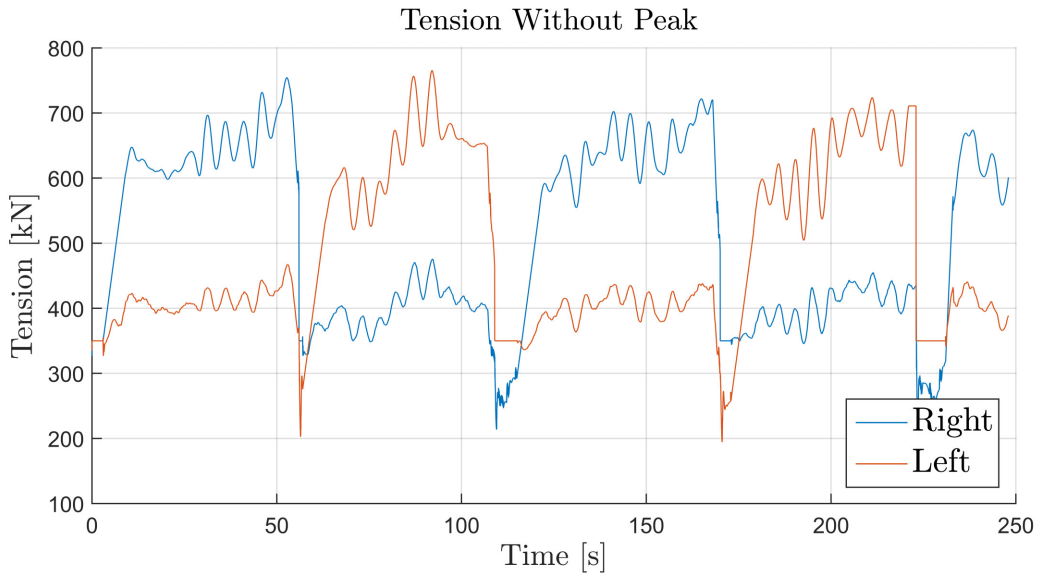


Figure 6.4: Tension Without Peak

Furthermore, the use of impulsive control to achieve a controlled breakaway force is shortly discussed by Geffen [9]. This means that an impulsive tension or velocity is given at the start, in order for the sawing wire in the wreck to start moving immediately. A faster increase of the tension will lower the break-away force that is needed as discussed by De Wit et al. [7]. This research is done with low forces, so the tests needs will need to be scaled up if possible.

### 6.3.1. Friction Compensation With PD control

After the sawing wire has started moving the dynamic friction in the system is governing. To be sure that the system does not fall back into static friction, PD control can be used. PD control makes use of a feedback system, since feed-foreword can cause for unexpected compensation. In the first case discussed for the elimination of the peak tension, the holding force at the beginning was lowered. The holding force is increased after the sawing wire has started moving. In order to make sure that this rise in tension does not cause for a slow down of the wire and possible static friction to occur, a PD controller can be used. When the system is controlled by a PD controller and the system is sufficiently stiff or damped, it will not experience sick-slip friction, as discussed by Geffen [9]. Use of PD control to avoid stick-slip friction is a common practice in other industries, especially for accurate machinery as described by Dupont [8]. More investigation to the application for high load systems should be done before implementation is possible.

## 6.4. Influence of the Heave Compensator

The effect of the heave compensator to reduce the tension in the wire was shown before in figure 5.5. The difference between the two graphs was calculated to be 21.5%, with an inclination angle of the sawing wire of 26 degrees. Changing the angle of the sawing wire to an average of 29 degrees makes the effect of the heave compensator larger, this is shown in figure 6.5. The effect is now increased to 22.8%. The result for an angle of 22 degrees is also shown in figure 6.5, with dotted lines showing the tension without heave compensation.

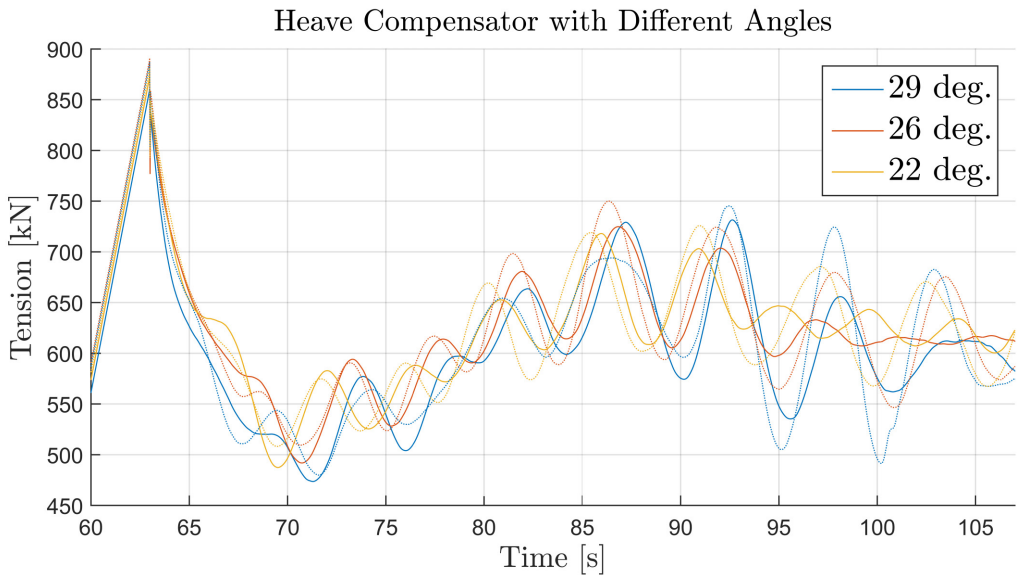


Figure 6.5: Heave Influence for Different Angles

The blue graphs give the simulation result of the steepest angle of the sawing wire. The steeper angle of the sawing wire also results in higher contact forces on the wreck, thanks to the decomposition of the forces. This makes the comparison in the figure unclear since higher angle also results in a larger amplitude. Therefore the error between the graphs is taken as a measurement of the heave compensation effect. The difference between the graphs with and without heave compensation is calculated using the root mean square of the signal as shown in equation 6.3. The results for three different sawing wire inclinations is shown in table 6.3.

$$RMS = \sqrt{mean(signal_1 - signal_2)^2} \tag{6.3}$$

| Inclination | Percentage |
|---|---|
| 22 deg. | 18.895 |
| 26 deg. | 21.488 |
| 29 deg. | 22.814 |

Table 6.3: Influence Heave Compensator

The influence of the heave compensator for the reduction of the tension is given for different angles of the sawing wire in figure 6.6. Here the influence of the surge motion is given as a cosine and the heave motion as a sine, to simulate the extension of the wire compared to the angle of the sawing wire. The yaw motion of the barges is not influenced by the inclination angle of the sawing wire but by the distance to the wreck and is therefore not included in the figure.

$$Heave = v_z \cdot sin(\theta)$$

$$Surge = v_x \cdot cos(\theta)$$

In these calculations, the mean velocity of the barge in heave and in surge motion was taken. The velocity graph of these motions is shown in figure 6.7. From the model results, it can be seen that the surge motion is around 1/3 the height of the heave motions. Therefore the influence graph for surge is lower. Furthermore, the values of the tension reduction that were shown in table 6.3 are shown in the graph as yellow crosses.

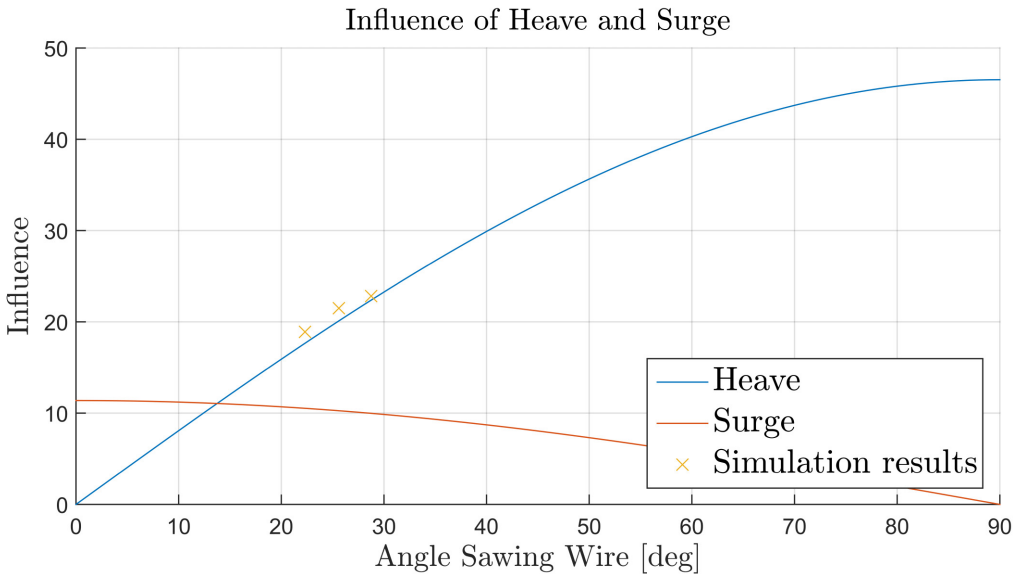


Figure 6.6: Influence of heave and surge

The steel wire inside the bushes will experience an increase of wear if the angle between the bushes gets too high, which is illustrated in figure 6.8. The graph of figure 6.6 is therefore misleading, since a higher angle than 30 percent is considered to inflict this increased wear of the wire, as stated in Tricolore [18].

Another aspect of the heave compensator assessed is focused on the horizontal motions of the barge. In the current model of the heave compensator, only the heave motion of the barges is taken into account. Though from the model it became clear that the surge and yaw motion of the barges also have a large influence on the tension in the wire. The surge motion is not easily included, so we will only continue to discuss the yaw motion in combination with the pitch motions. The complete elongation of the wire can be described by formula 6.4, is called the unit vector.

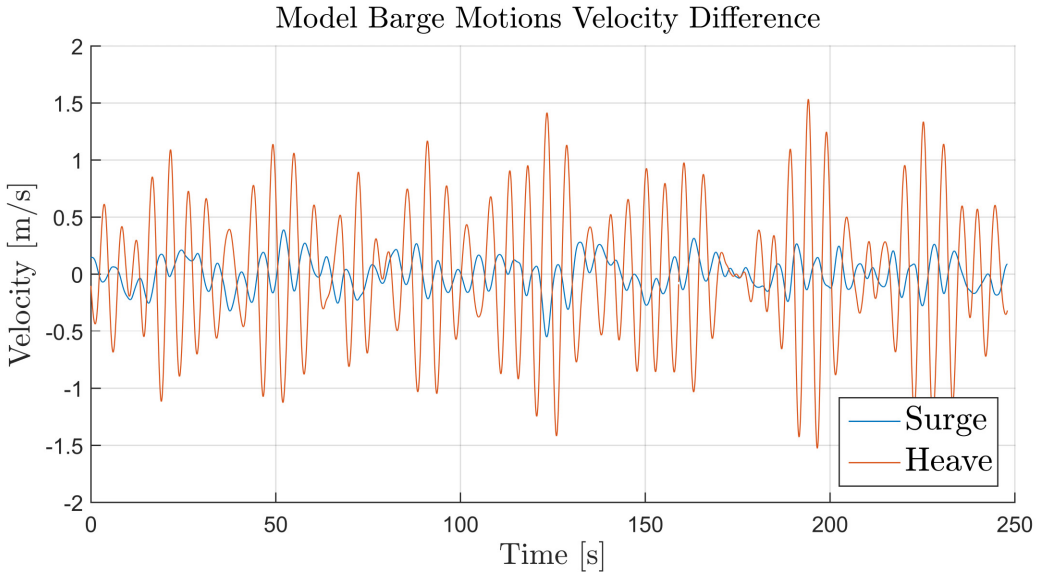


Figure 6.7: Barge Velocity Surge/Heave

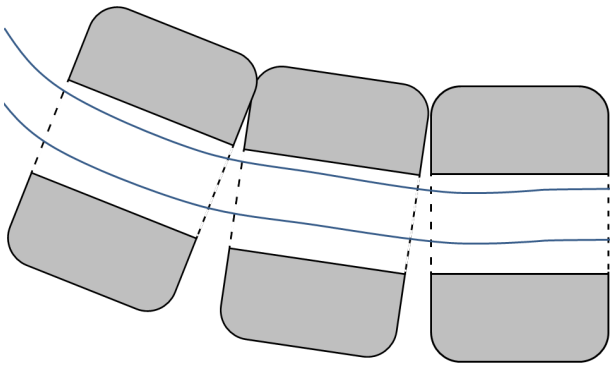

Figure 6.8: Bending of the wire inside bushes

$$\gamma = \begin{Bmatrix} x \\ y \\ z \end{Bmatrix} = \begin{Bmatrix} \cos(\text{yaw}) \cdot cos(pitch) \\ \sin(\text{yaw}) \cdot cos(pitch) \\ \text{-sin(pitch)} \end{Bmatrix} \tag{6.4}$$

For now, the model has a very narrow directional spreading, therefore it is not influenced much by the yaw motion of the barge much. This will need to be adjusted in order to see the extra effect of the improved heave compensator, with the unit vector included.

## 6.5. Conclusions

Accidental load scenarios were assessed which showed similar results for the simulation for wave height $H_s = 1.5[m]$ and a draft of 4,76 [m]. Other things to notice is the setting for winch velocity and tension. This is regulated by the installed power, since the velocity should be kept with a certain tension. The trade-off between installed power and sawing speed is interesting for future operations, but should be researched further. Further on the implementation of the system in future operations, it is assessed what the influence of a bigger

or smaller diameter or a different material would have to the system. From this, it could be concluded that the bigger diameter would result in a higher friction force because of the larger contact area. The material such as concrete would probably result in lower pulling force since its coefficient of friction is smaller. Though the coefficient of friction should be tested for the abrasive cutting process between the steel bushes and concrete. In future operations, it can be interesting to decrease of eliminate the breakaway force peak shown in the beginning of a sawing cycle. For example, the mean breaking load of the sawing wire is calculated with this highest peak load. The required power in the system also showed a similar peak at the beginning of the sawing cycle, so if this could be lowered it would have a profound affect. The lowering of this peak tension force can be done by lowering the holding force at the start of the sawing cycle and increasing it afterward, or by applying impulsive control. Further testing will need to be conducted to validate the effect on the peak tension force, especially since the theory is mostly concentrated on smaller machinery systems. Regarding the heave compensator, it is advised to place the barges closer to the wreck to increase the effect of the heave compensator the reduction of the tension. The closer placement will increase the sawing wire angle from 25 to 30 percent. The angle described is limited since the amount of required lateral forces needs to be reached and the internal bending of the steel wire inside of the bushes may cause additional wear at steeper angles. Another way to increase the effect of the heave compensator is by extending the compensation for motions in the z direction by adding x and y directions. If the yaw motion is measured this could be included in the heave compensator controller, this can be done with a unit vector. The velocity of surge and heave of the barges is measured in the model, they show a difference of $\frac{1}{3}$.

# 7

# Conclusions and recommendations

The objective of this research thesis is to contribute to the design assessment of the sawing wire system by providing a simulation model and comparing this to the measurements made during the salvage operation of the Baltic Ace. This has been achieved and in this chapter the results of the research will be concluded.

## 7.1. Conclusions

First starting with the measurements, these were analyzed and compared with fiction theory. The first conclusions could be made:

- The measurements of the sawing wire operation show peak tensions in the beginning of a sawing cycle. These peaks are called the breakaway force which is required to get the sawing wire moving. The peak is caused by the difference in the static and kinetic friction coefficients and is generally $20-30\%$ higher compared to the constant tension part. When the velocity of the winch is compared with the tension it is clear that the tension peak takes place before the sawing wire is moving. This answers the first central research question:"Where do the high tension peaks at the beginning of a sawing cycle originate from".

- Secondly the stick-slip friction is taken into account in the sawing wire simulation by use of the Stribeck friction model. The stick-slip phenomenon occurs when the velocity of the wire falls back and the friction coefficient comes close to the static friction coefficient. This causes for intermittent movement of the sawing wire. The first sub-question: "What is stick-slip friction and is this present?", is answered and the stick-slip phenomena should be included in the model.

- The tension forces of the winches are much higher compared to the equivalent forces created by the weight of the sawing wire. The sawing wire inertia is therefore not considered to play a significant part in the creation of the peak tension in the beginning of the sawing cycle, thus answering the second sub-question:"What is the influence of inertia in the system?".

- The friction coefficient for the sawing of the Baltic Ace was calculated by dividing the lateral forces by the normal forces. This was applied to the measurements, resulting in average values for the static friction coefficient of 1 and the dynamic friction coefficient of 0.8. Similar values were found in theory and previous cutting off the Tricolore. Therefore these values can be used for the friction of a shipwreck, which is the answer to the second central research question: "What is the friction coefficient that can be used for the simulation of a shipwreck?".

The simulation model of the sawing wire system has been made in the program Orcaflex. Therefore the first part of the objective is achieved and some conclusions to the model are made next:

- The friction in the wreck is covered by a shape in Orcaflex with a coefficient of friction and an extra damper on both sides of the sawing wire that includes the stick-slip friction. The difference between static and kinetic friction is covered by an extra tension at low velocities. This answers the third central research question: "How can we include different friction coefficients in a model?".

- The heave compensators are inserted as a winch on top of the barges. The required stroke of the heave compensator is calculated in an external code in phyton. In this code, the angular pitch velocity of the barges at the fairlead position is multiplied by the sinus of the declination angle of the sawing wire. This answers the third sub-question: "How is the heave motion of the barges compensated?".

The results of the model have been compared with the measurements. With this comparison the following conclusions could be made:

- The tension of the model and the measurements are comparable. The peaks that are shown in a longer time-trace sometimes have higher or lower peaks, but generally do not vary much. The frequency domain comparison of the model and the measurements show very similar energy peaks in the lower frequencies. Therefore the model is considered to be a correct representation of the sawing procedure.
- The heave compensator as modeled in the model shows a reduction of the tension amplitude when it is turned on compared to a model where it is turned off. The breakaway force in the beginning of the sawing cycles is not compensated with the heave compensator, since this is not caused by the movement of the barges but by friction. The velocity graph shows that the heave compensator sometimes requires a higher or lower velocity of the winch in order to compensate for the barge motions.

## 7.2. Recommendations

The recommendations are mostly focused on the future implementation of the sawing wire system.

- The trade-off between installed power and sawing speed is researched only little for this report, though for future operations it would be interesting to look further into this.
- In the design assessment, it was considered to implement the system for a smaller or bigger wreck of a concrete tunnel. A bigger diameter wreck would result in a higher friction force because of the larger contact area. But for the change of material is more difficult to predict the friction forces. Most likely this will result in lower pulling forces, since its coefficient of friction is smaller. Though the coefficient of friction should be tested for the abrasive cutting process between the steel bushes and concrete.
- Lowering of the peak tension force can be done by lowering the holding force at the start of the sawing cycle and increasing it afterward, or by applying impulsive control. Further testing will need to be conducted to validate the effect on the peak tension force, especially since the theory is mostly concentrated on smaller machinery systems.
- Regarding the heave compensator it is advised to place the barges closer to the wreck to increase the effect of the heave compensator to reduce the tension. The closer placement will increase the sawing wire angle from 25 to 30 percent. The angle described is limited since the amount of required lateral forces needs to be reached and the internal bending of the steel wire inside of the bushes may cause additional wear at steeper angles.
- Another way to increase the effect of the heave compensator is by extending the compensation for motions in the z direction by adding x and y directions. If the yaw motion is measured this could be included in the heave compensator controller, this can be done with a unit vector.

# A

# Appendix-A

| Stage | Stage duration (s) | Simulation Time (s) | Mode | Value | Unit |
|---|---|---|---|---|---|
| Statics | | | Specified Length | 15 | m |
| 0 | 3 | 0 | Specified Tension | 300 | kN |
| 1 | 3 | 3 | Specified Payout Rate | 0 | m/s |
| 2 | 6 | 9 | Specified Tension | 300 | kN |
| 3 | 45 | 54 | Specified Tension | 300 | kN |
| 4 | 2 | 56 | Specified Tension | 300 | kN |
| 5 | 1 | 57 | Specified Payout Rate | 0 | m/s |
| 6 | 6 | 63 | Specified Payout Rate Change | -0.8 | m/s |
| 7 | 44 | 107 | Specified Payout Rate | -0.8 | m/s |
| 8 | 2 | 109 | Specified Payout Rate Change | 0.8 | m/s |
| 9 | 6 | 115 | Specified Payout Rate | 0 | m/s |
| 10 | 6 | 121 | Specified Tension | 300 | kN |
| 11 | 47 | 168 | Specified Tension | 300 | kN |
| 12 | 2 | 170 | Specified Tension | 300 | kN |
| 13 | 3 | 173 | Specified Payout Rate | 0 | m/s |
| 14 | 6 | 179 | Specified Payout Rate Change | -0.8 | m/s |
| 15 | 42 | 221 | Specified Payout Rate | -0.8 | m/s |
| 16 | 2 | 223 | Specified Payout Rate Change | 0.8 | m/s |
| 17 | 8 | 231 | Specified Payout Rate | 0 | m/s |
| 18 | 2 | 233 | Specified Tension | 300 | kN |
| 19 | 15 | 248 | Specified Tension | 300 | kN |

Table A.1: Left winch settings

| Stage | Stage duration (s) | Simulation Time (s) | Mode | Value | Unit |
|---|---|---|---|---|---|
| Statics | | | Specified Tension | 300 | kN |
| 0 | 3 | 0 | Specified Tension | 300 | kN |
| 1 | 3 | 3 | Specified Payout Rate | 0 | m/s |
| 2 | 6 | 9 | Specified Payout Rate Change | -0.8 | m/s |
| 3 | 45 | 54 | Specified Payout Rate | -0.8 | m/s |
| 4 | 2 | 56 | Specified Payout Rate Change | 0.8 | m/s |
| 5 | 1 | 57 | Specified Payout Rate | 0 | m/s |
| 6 | 6 | 63 | Specified Tension | 300 | kN |
| 7 | 44 | 107 | Specified Tension | 300 | kN |
| 8 | 2 | 109 | Specified Tension | 300 | kN |
| 9 | 6 | 115 | Specified Payout Rate | 0 | m/s |
| 10 | 6 | 121 | Specified Payout Rate Change | -0.8 | m/s |
| 11 | 47 | 168 | Specified Payout Rate | -0.8 | m/s |
| 12 | 2 | 170 | Specified Payout Rate Change | 0.8 | m/s |
| 13 | 3 | 173 | Specified Payout Rate | 0 | m/s |
| 14 | 6 | 179 | Specified Tension | 300 | kN |
| 15 | 42 | 221 | Specified Tension | 300 | kN |
| 16 | 2 | 223 | Specified Tension | 300 | kN |
| 17 | 8 | 231 | Specified Payout Rate | 0 | m/s |
| 18 | 2 | 233 | Specified Payout Rate Change | -0.8 | m/s |
| 19 | 15 | 248 | Specified Payout Rate | -0.8 | m/s |

Table A.2: Right winch settings

| Stage | Stage duration (s) | Simulation Time (s) | Mode | Value | Unit |
|---|---|---|---|---|---|
| Statics | | | Specified Length | 10 | m |
| 0 | 3 | 0 | Specified Payout Rate | 0 | m/s |
| 1 | 3 | 3 | Specified Tension | 350 | kN |
| 2 | 6 | 9 | Specified Payout Rate | 0 | kN |
| 3 | 45 | 54 | Length at Stage End | 10 | m |
| 4 | 2 | 56 | Specified Payout Rate | 0 | m/s |
| 5 | 1 | 57 | Length at Stage End | 10 | m |
| 6 | 6 | 63 | Specified Tension Change | 600 | kN |
| 7 | 44 | 107 | Specified Payout Rate | 0 | m/s |
| 8 | 2 | 109 | Specified Payout Rate | 0 | m/s |
| 9 | 6 | 115 | Specified Tension | 350 | kN |
| 10 | 6 | 121 | Specified Payout Rate | 0 | m/s |
| 11 | 47 | 168 | Length at Stage End | 10 | m |
| 12 | 2 | 170 | Specified Payout Rate | 0 | m/s |
| 13 | 3 | 173 | Length at Stage End | 10 | m |
| 14 | 6 | 179 | Specified Tension Change | 600 | kN |
| 15 | 42 | 221 | Specified Payout Rate | 0 | m/s |
| 16 | 2 | 223 | Specified Tension Change | 0 | m/s |
| 17 | 8 | 231 | Specified Tension | 350 | kN |
| 18 | 2 | 233 | Specified Payout Rate | 0 | m/s |
| 19 | 15 | 248 | Specified Payout Rate | 0 | m/s |

Table A.3: Left Tensioner settings

| Stage | Stage duration (s) | Simulation Time (s) | Mode | Value | Unit |
|---|---|---|---|---|---|
| Statics | | | Specified Length | 10 | m |
| 0 | 3 | 0 | Specified Payout Rate | 0 | m/s |
| 1 | 3 | 3 | Specified Tension | 350 | kN |
| 2 | 6 | 9 | Specified Tension Change | 600 | kN |
| 3 | 45 | 54 | Specified Payout Rate | 0 | m/s |
| 4 | 2 | 56 | Specified Payout Rate | 0 | m/s |
| 5 | 1 | 57 | Specified Tension | 350 | kN |
| 6 | 6 | 63 | Specified Payout Rate | 0 | m/s |
| 7 | 44 | 107 | Length at Stage End | 10 | m |
| 8 | 2 | 109 | Specified Payout Rate | 0 | m/s |
| 9 | 6 | 115 | Length at Stage End | 10 | m |
| 10 | 6 | 121 | Specified Tension Change | 600 | kN |
| 11 | 47 | 168 | Specified Payout Rate | 0 | m/s |
| 12 | 2 | 170 | Specified Payout Rate | 0 | m/s |
| 13 | 3 | 173 | Specified Tension | 350 | kN |
| 14 | 6 | 179 | Specified Payout Rate | 0 | m/s |
| 15 | 42 | 221 | Length at Stage End | 10 | m |
| 16 | 2 | 223 | Specified Payout Rate | 0 | m/s |
| 17 | 8 | 231 | Length at Stage End | 10 | m |
| 18 | 2 | 233 | Specified Tension Change | 600 | kN |
| 19 | 15 | 248 | Specified Payout Rate | 0 | m/s |

Table A.4: Right Tensioner settings

# B

# Appendix-B

```
"""
This model controlles the heave compensator connected to the left barge.
The velocity of the fairlead on the barge is measured and multiplied with the sin
of the wire angle to get the payout veolicty
"""
import math
class PIDstate(object):
    def __init__(self):
        self.valid = False
        self.time = -OrcFxAPI.OrcinaInfinity()
        self.signal = 0.0
        self.iedt = 0.0
        self.dedt = 0.0

    def getStateAttributes(self):
        return {
            'valid': self.valid,
            'time': self.time,
            'signal': self.signal,
            'iedt': self.iedt,
            'dedt': self.dedt
        }

    def setStateAttributes(self, attributes):
        self.valid = attributes['valid']
        self.time = attributes['time']
        self.signal = attributes['signal']
        self.iedt = attributes['iedt']
        self.dedt = attributes['dedt']

change = range(0,15,1)
class PIDController(object):

    def Initialise(self, info):
        # In the Calculate() method we'll need to ask OrcaFlex for the value of
        # our controlled variable. To do this we'll need an OrcFxAPI.Period to say
        # we want the value 'now':
        self.periodNow = OrcFxAPI.Period(OrcFxAPI.pnInstantaneousValue)
```

```
        # And we'll need an ObjectExtra saying we want the value at the origin
        # of the controlled object:
        self.ObjectExtra = OrcFxAPI.ObjectExtra()
        self.ObjectExtra.RigidBodyPos = (0.0, 0.0, 0.0)

        # Set up a convenient function to get values from the info.ObjectParameters
        # that is passed by OrcaFlex. This contains a dictionary containing the
        # parameters specified on the External Functions page of the winch data form:
        params = info.ObjectParameters
        def GetParameter(paramName, default=None):
            if paramName in params:
                param = params[paramName]
                if isinstance(default, float):
                    param = float(param)
                elif isinstance(default, int):
                    param = int(param)
            elif not default is None:
                param = default
            else:
                raise Exception('Parameter %s is required but is not included in the object para
            return param

        # Now use GetParameter to get the various parameters that are specified
        # on the External Functions page in the OrcaFlex model:
        # Name of model object whose result variable is to be controlled:
        self.ControlledObject = info.Model[GetParameter('ControlledObject')]
        self.ControlledObject2 = info.Model[GetParameter('ControlledObject2')]
        self.ControlledObject3 = info.Model[GetParameter('ControlledObject3')]
##          self.ControlledObject4 = info.Model[GetParameter('ControlledObject4')]
##          self.ControlledObject5 = info.Model[GetParameter('ControlledObject5')]
        self.DetailedWinchOposite = info.Model['Winch Velocity Right']
        self.DetailedWinch = info.Model['Winch Velocity Left']
        # The result variable of that object to be controlled. This must be
        # one of the results available for the ControlledObject on the results
        # form in OrcaFlex:
        self.ControlledVariable = GetParameter('ControlledVariable')
        self.ControlledVariable2 = GetParameter('ControlledVariable2')
        self.ControlledVariable3 = GetParameter('ControlledVariable3')
##          self.ControlledVariable4 = GetParameter('ControlledVariable4')
##          self.ControlledVariable5 = GetParameter('ControlledVariable5')
        # The target value for that controlled variable. Its units are those of
        # that controlled variable in the OrcaFlex model:
        self.TargetValue = GetParameter('TargetValue', 0.0)
        # The constants of the PID controller:
        self.k0 = GetParameter('k0', 0.0) # constant part
        self.kP = GetParameter('kP', 0.0) # scaling constant for the proportional part
        self.kI = GetParameter('kI', 0.0) # scaling constant for the integral part
        self.kD = GetParameter('kD', 0.0) # scaling constant for the differential part
        # If no value of ControlStartTime is specified then default to -Infinity,
        # so that we activate control at the start of the simulation:
        self.ControlStartTime = GetParameter('ControlStartTime', -OrcFxAPI.OrcinaInfinity())
        # And default to not limiting the control variable:
        self.MinValue = GetParameter('MinValue', -OrcFxAPI.OrcinaInfinity())
        self.MaxValue = GetParameter('MaxValue', OrcFxAPI.OrcinaInfinity())

        # If info.StateData is not None then we have been called when loading
```

```
        # a simulation, so we need to restore the controller state
        # to what our StoreState() method saved when the simulation was stored:
        self.prev = PIDstate()
        self.now = PIDstate()
        if info.StateData:
            import json
            state = json.loads(info.StateData)
            self.now.setStateAttributes(state['now'])
            self.prev.setStateAttributes(state['prev'])
        else:
            # This is a new simulation, so initialise the controller state:
            self.prev.iedt = GetParameter('Initial e/D', 0.0)
            self.now.dedt = GetParameter('Initial De', 0.0)

        print('Initialised OK.')

    def Calculate(self, info):
        # Don't start control until the specified time:
        if info.SimulationTime < self.ControlStartTime:
            return

        # If this is a new time step, and not the first, then step self.now back
        # to become our new self.prev:
        if info.NewTimeStep and self.now.valid:
            self.prev.time = self.now.time
            self.prev.signal = self.now.signal
            self.prev.signal2 = self.now.signal2
            self.prev.iedt = self.now.iedt
            self.prev.dedt = self.now.dedt
            self.prev.valid = True

        # Get the state values now:
        self.now.time = info.SimulationTime
        self.now.signal = self.ControlledObject.TimeHistory(
          self.ControlledVariable,
          self.periodNow, # set up in Initialise() method to give the value 'now'
          self.ObjectExtra # set up in Initialise() method
        )[0] # TimeHistory returns an array, which in this case contains just 1 item, the value now
##          self.now.signal = self.now.signal/0.35
        self.now.iedt = self.prev.iedt
        self.now.valid = True

        # Get the state values now:

        self.now.signal2 = self.ControlledObject2.TimeHistory(
          self.ControlledVariable2,
          self.periodNow, # set up in Initialise() method to give the value 'now'
          self.ObjectExtra # set up in Initialise() method
        )[0] # TimeHistory returns an array, which in this case contains just 1 item, the value now
##          self.now.signal = self.now.signal/0.35
        self.now.iedt = self.prev.iedt
        self.now.valid = True

        self.now.angle3 = self.ControlledObject3.TimeHistory(
          self.ControlledVariable3,
          self.periodNow, # set up in Initialise() method to give the value 'now'
```

```
            self.ObjectExtra # set up in Initialise() method
        )[0] # TimeHistory returns an array, which in this case contains just 1 item, the value
##          self.now.signal = self.now.signal/0.35
        self.now.iedt = self.prev.iedt
        self.now.valid = True

##          self.now.signal4 = self.ControlledObject4.TimeHistory(
##            self.ControlledVariable4,
##            self.periodNow, # set up in Initialise() method to give the value 'now'
##            self.ObjectExtra # set up in Initialise() method
##          )[0] # TimeHistory returns an array, which in this case contains just 1 item, the valu
####          self.now.signal = self.now.signal/0.35
##          self.now.iedt = self.prev.iedt
##          self.now.valid = True
##
##          self.now.angle5 = self.ControlledObject5.TimeHistory(
##            self.ControlledVariable5,
##            self.periodNow, # set up in Initialise() method to give the value 'now'
##            self.ObjectExtra # set up in Initialise() method
##          )[0] # TimeHistory returns an array, which in this case contains just 1 item, the valu
####          self.now.signal = self.now.signal/0.35
##          self.now.iedt = self.prev.iedt
##          self.now.valid = True


        angle65 = math.radians(self.now.angle3)
        angle25 = math.radians(90-self.now.angle3)
##          angley = math.radians(self.now.angle5)
        e  = self.now.signal
        ee = self.now.signal2
        info.Value = e*math.sin(angle25)*-45
#          info.Value = e*math.sin(angle25) -ee*math.cos(angle25)
##          info.Value = e*math.sin(angle25) -ee*math.cos(angle25) +math.fabs(self.now.signal4*mat



    def StoreState(self, info):
        # The simulation is being stored, so we need to store our controlled state
        # to the simulation file so that when the simulation is re-loaded our
        # Initialise() method can restore to the same state. We use the built json module to get
        # the controller state into a form suitable for putting into info.StateData,
        # which OrcaFlex will store in the simulation file for us:
        import json
        state = {'now': self.now.getStateAttributes(), 'prev': self.prev.getStateAttributes()}
        info.StateData = json.dumps(state)
```

# C

# Appendix-C

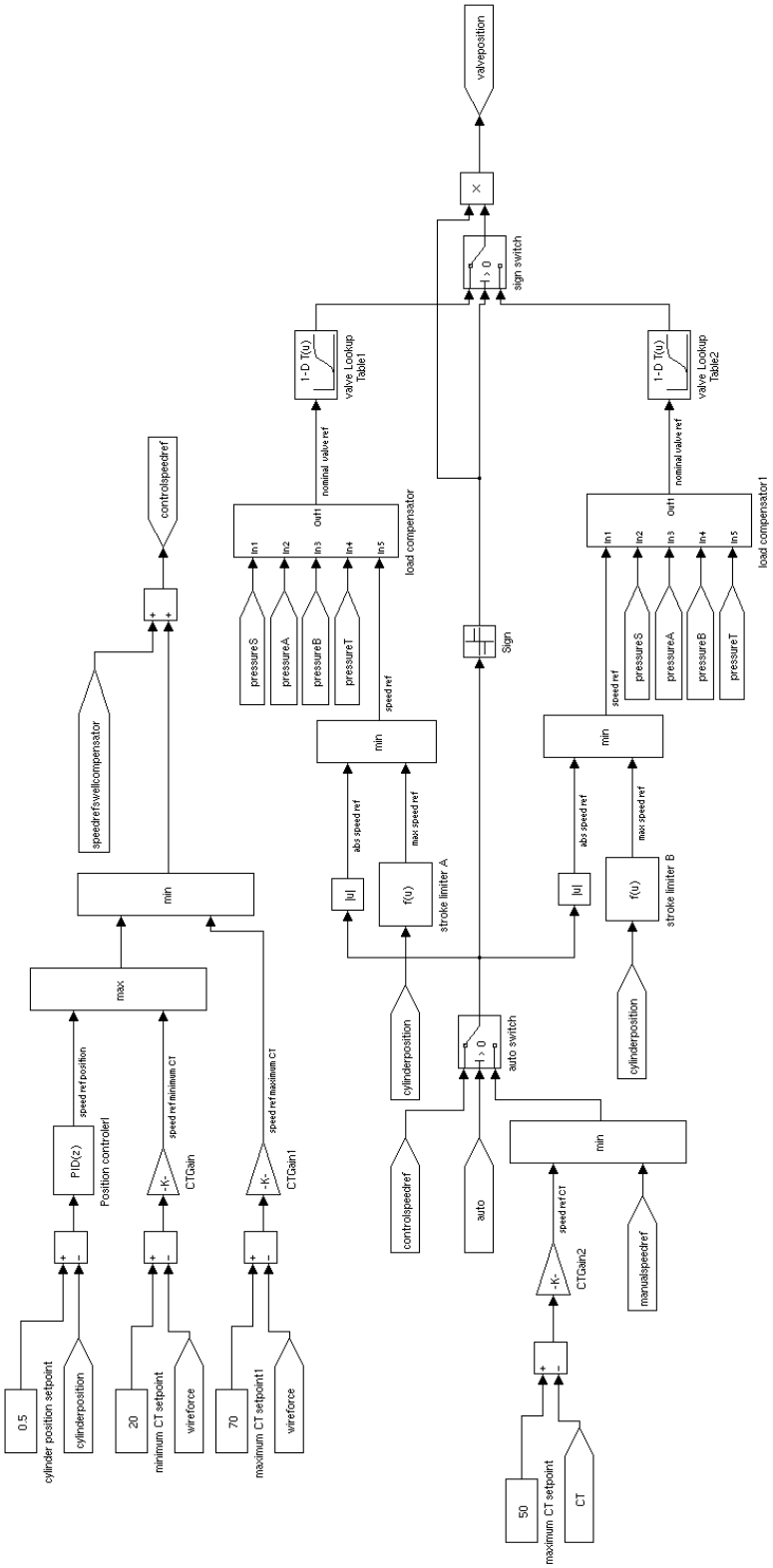


Figure C.1: heave compensator scheme

# D

# Appendix-D

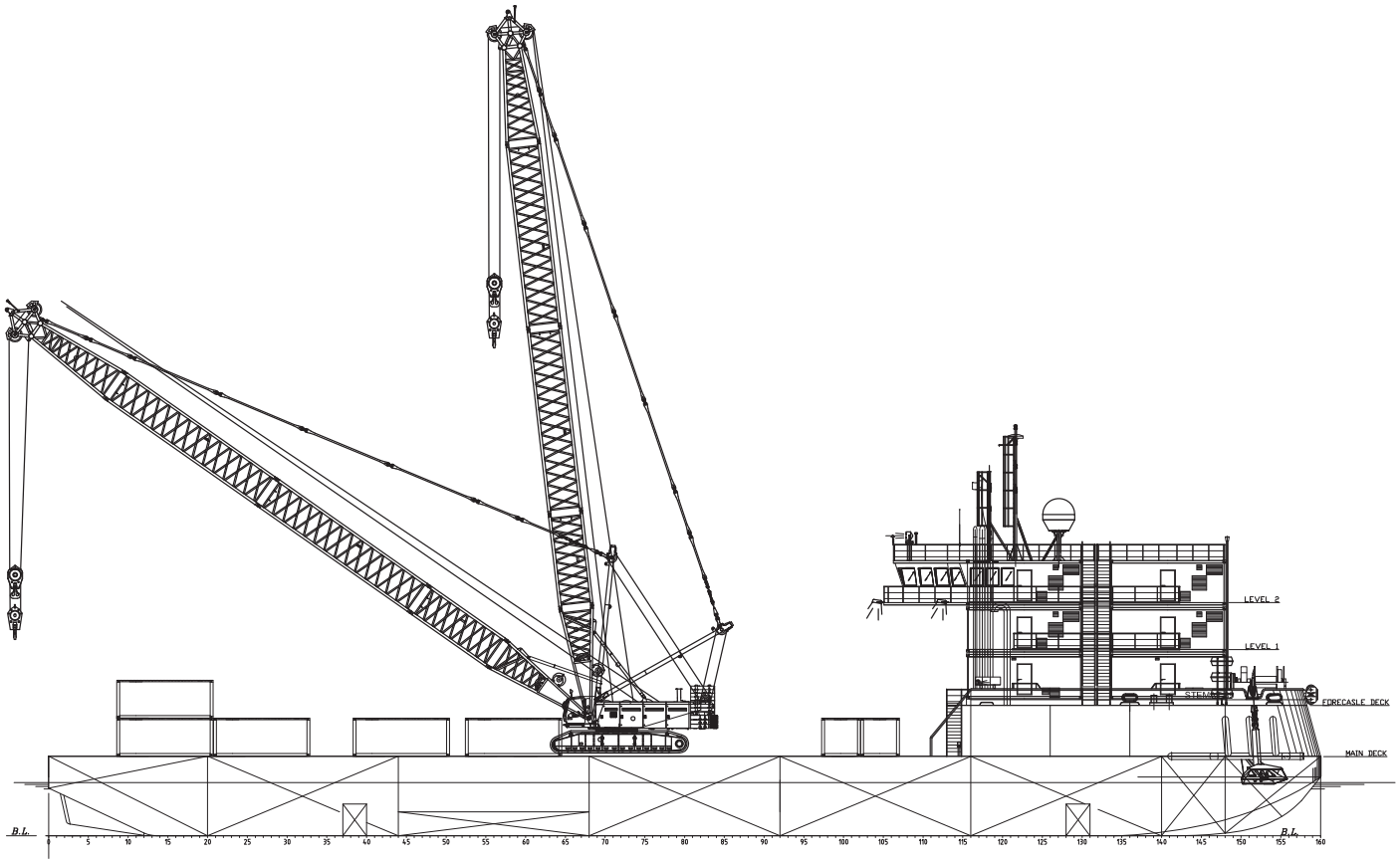


SECTION 7000 OFF CL. S.B.

"Stemat 89"
Lengte : 80 m
Breedte : 24 m
Hoogte : 5 m

| Rev | Date | Drawn | Description | Chkd | P.Appr | E.Appr | Client | Date |
|---|---|---|---|---|---|---|---|---|
| B | DD-MMM-YY | JWOL | FOR CLIENT'S REVIEW | GVEH | PHH | PKOR | | |
| A | 02-10-2014 | JWOL | FOR INTERNAL REVIEW | GVEH | PHH | PKOR | | |

Subject: DECKLAYOUT "STEMAT 89"
SECTION 7000 OFF CL. S.B.

Project: BALTIC ACE WRECK REMOVAL NOORDZEE

Client: SMIT SALVAGE

Boskalis OFFSHORE ENGINEERING DEPARTMENT
P.O.Box 43, 3350 AA Papendrecht
E-mail: info@boskalis.nl

CAD-drwg not to be changed manually

Orig. Size A3



| Scale | Drawing No | Sheet |
|---|---|---|
| 1:300 | OE14AC011-D-202 | 3 of 4 |

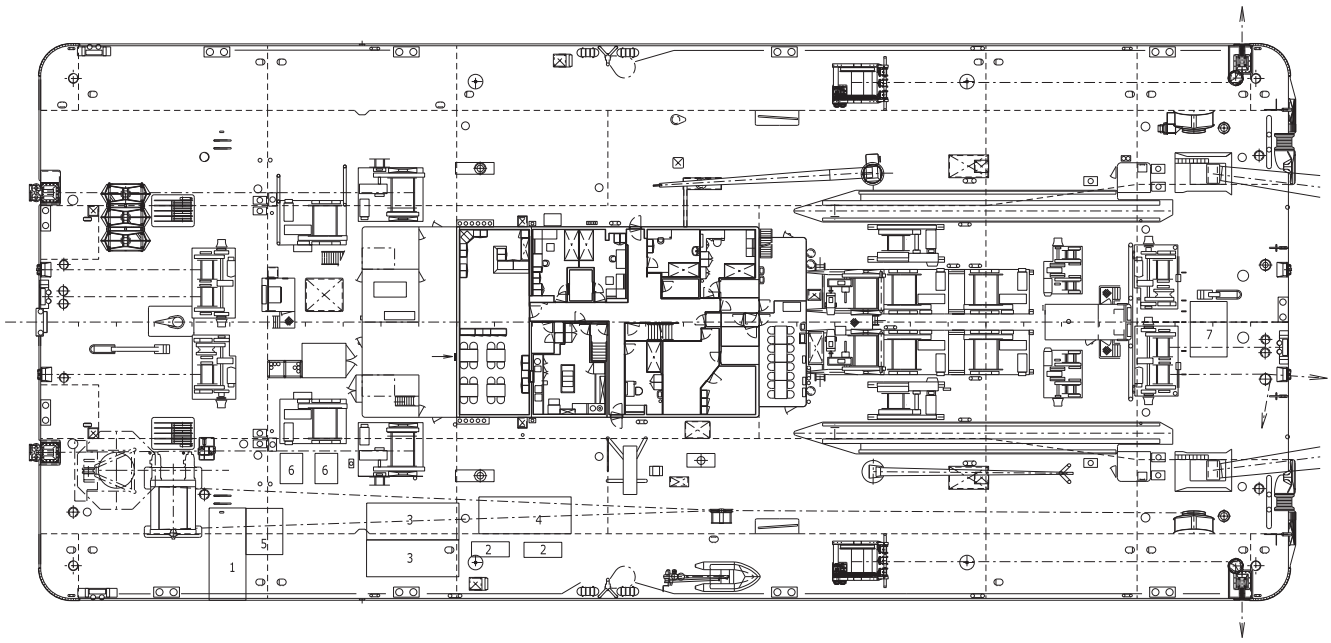


1. A-FRAME
2. 150 kVA GENERATOR
3. DECOMPRESSION CHAMBER
4. COMPRESSOR CONTAINER
5. DIVE CONTROL
6. HPU
7. UMBILICALWINCH GRAB

PRELIMINARY

SCALE IN METRES

0 2.5 5 7.5 10 12.5

| Rev | Date | Drawn | Description | Chkd | P.Appr | E.Appr | Client | Date |
|---|---|---|---|---|---|---|---|---|
| B | 19-03-2014 | ATER | FOR CLIENT'S REVIEW | GYEH | JEIA | PKOR | | |
| A | 19-03-2014 | ATER | FOR INTERNAL REVIEW | GYEH | JEIA | PKOR | | |

Subject: DECK LAYOUT TAKLIFT 4

Project: Baltic Ace wreckremoval

Client: SMIT Salvage

Boskalis OFFSHORE ENGINEERING DEPARTMENT
P.O.Box 43, 3350 AA Papendrecht
E-mail: info@boskalis.nl

CAD-drwg not to be changed manually

Orig. Size A3



| Scale | Drawing No | Sheet |
|---|---|---|
| 1:250 | OE14AC011-D-203 | 1 of 1 |

**Stemat barge**

Figure D.1: Stemat 89

| **Specifications Stemat 89** | |
|---|---|
| Draught | 3m |
| Displacement weight | 7604 Ton |
| Length | 80m |
| Breadth | 24m |
| Depth | 5 m |
| Kxx | 9m |
| Kyy | 23.6m |
| Kzz | 24.24m |

Table D.1: Specifications Stemat 89

### Mammoet barge


Figure D.2: MSB3301

| Specifications Mammoet MSB3301 | |
|---|---|
| Draught | 3m |
| Displacement weight | 7815 Ton |
| Length | 100.5m |
| Breadth | 30.5m |
| Depth | 6.1 m |
| Kxx | 9m |
| Kyy | 25.3m |
| Kzz | 27.02m |

Table D.2: Specifications MSB3301

### Stemat Barge

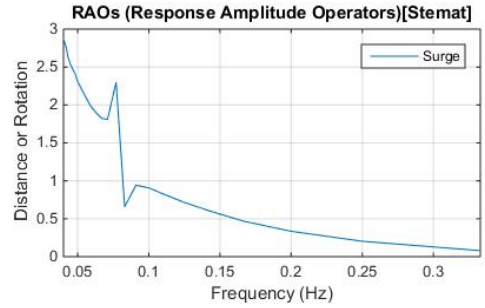


(a) Surge

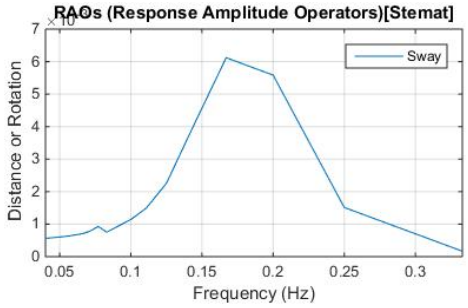


(b) Sway

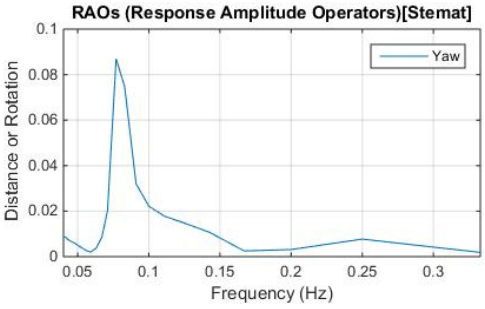


(c) Yaw

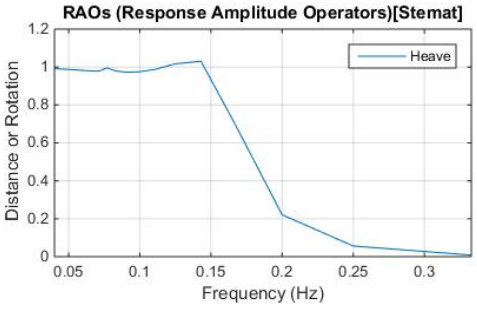


(d) Heave

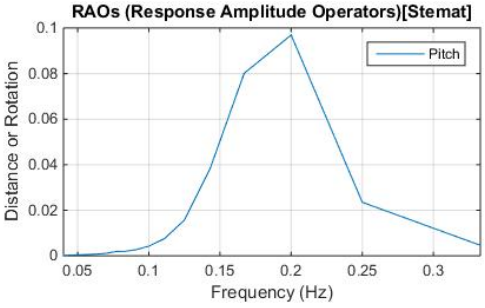


(e) Pitch

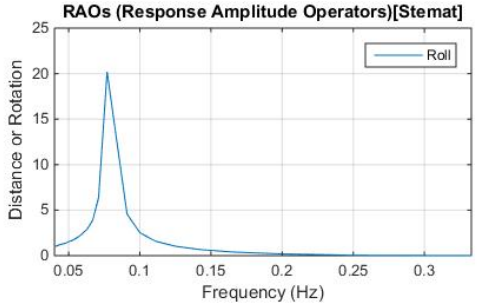


(f) Roll

Figure D.3: RAO Stemat barge

**MSB barge**

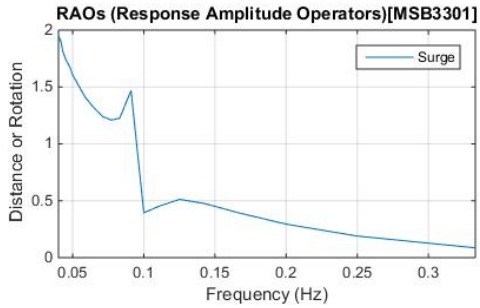


(a) Surge

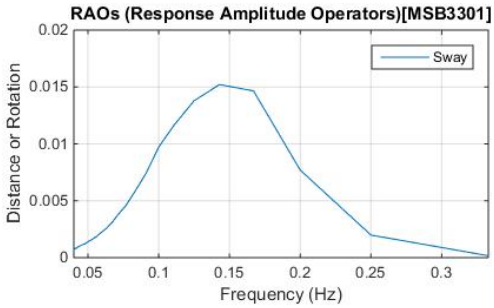


(b) Sway

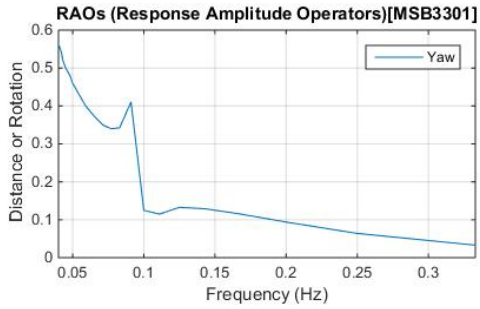


(c) Yaw

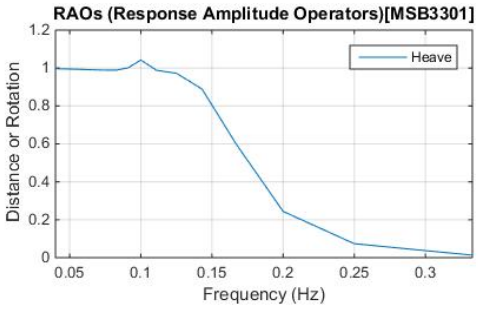


(d) Heave

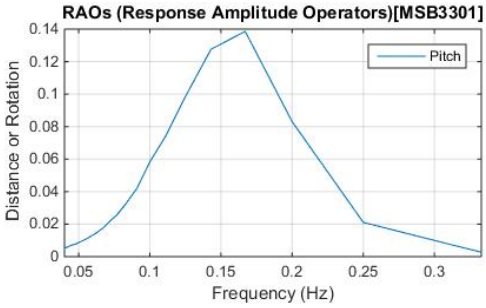


(e) Pitch

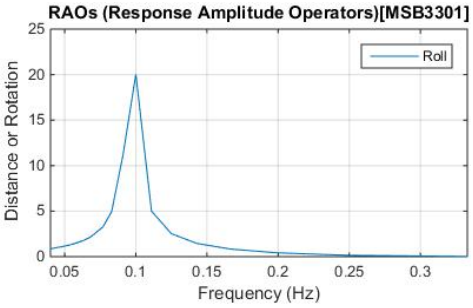


(f) Roll

Figure D.4: RAO Stemat barge

# Bibliography


[1] Andersson, S., Soerberg, A., and Bjoklund, S. (2007). Friction models for sliding dry, boundary and mixed lubricated contacts. *Tribology International*, 40:580–587.

[2] Bhushan, B. (2013). *Introduction to Tribology, Second Edition*.

[3] Boskalis (2014). Winch motion analysis max tension. Technical report.

[4] Boskalis (2015). Uitvoeringsplan 2015. Technical report.

[5] Boskalis and Mammoet Salvage (2015). Deelkwaliteitplan Ankerplan. Technical report.

[6] Briscoe, B. (1992). Tribology — Friction and wear of engineering materials.

[7] De Wit, C. C., Olsson, H., Astrom, K. J., and Lischinsky, P. (1995). A new model for control of systems with friction. *Automatic Control, IEEE Transactions on*, 40(3):419–425.

[8] Dupont, P. E. (1994). Avoiding sitck-slip Through PD control.

[9] Geffen, V. V. (2009). A study of friction models and friction Compensation. Technical report, Technische Universiteit Eindhoven, Eindhoven.

[10] Holthuijsen, L. H. (2007). *Waves in oceanic and coastal waters*. Cambridge University Press, New York.

[11] Huisman Equipment (2013). Wiresaw simulation. Technical report.

[12] Journée, J. M. J. and Massie, W. W. (2001). OFFSHORE HYDROMECHANICS.

[13] Mammoet Salvage, B. (2010). MSB 3301. Technical Report 7152013.

[14] Morphett, A. L., Crawford, C. M., Chiro, B., and Lee, D. (2010). Motion analysis of pontoon stemat 82. Technical report.

[15] Osgood, B. (2010). The Fourier Transform and its Applications - Lecture Notes. Technical report, Stanford University.

[16] Rabbat, B. G. and Russell, H. G. (1985). Friction Coefficient of Steel on Concrete or Grout TT -. *Journal of Structural Engineering TA -*, 111(3):505–515.

[17] Straffelini, G. (2015). *Friction and Wear*.

[18] Tricolore, C. B. (2010). Zaag verslag Tricolore.

[19] van Campen, D. H., de Kraker, a., van den Steen, L., and Leine, R. I. (1998). Stick-Slip Vibrations Induced by Alternate Friction Models. *Nonlinear Dynamics*, 16:41–54.

[20] Van de Vrande, B. L., Van Campen, D.H., and De Kraker, A. (2010). Some Aspects of the Analysis of Stick-Slip Vibrations with an Application to Drill Strings. Technical report, Eindhoven University of Technology, Department of Mechanical Enggineering, Eindhoven.

[21] Veritas, B. (2010). Stemat 82 specifications. Technical Report 0.